Active Target Tracking and Cooperative Localization for Teams of Aerial Vehicles

Fabio Morbidi, *Member, IEEE*, and Gian Luca Mariottini, *Member, IEEE*

Abstract—This paper studies the active target-tracking problem for a team of unmanned aerial vehicles equipped with 3-D range-finding sensors. We propose a gradient-based control strategy that encompasses the three major optimum experimental design criteria, and we use the Kalman filter for estimating the target's position both in a *cooperative* and in a *noncooperative* scenario. Our control strategy is *active* because it moves the vehicles along paths that minimize the uncertainty about the location of the target. In the case that the position of the vehicles is not perfectly known, we introduce a new and more challenging problem, termed *active cooperative localization and multitarget tracking* (ACLMT). In this problem, the aerial vehicles must reconfigure themselves in the 3-D space in order to maximize both the accuracy of their *own position estimate* and that of *multiple moving targets*. For ACLMT, we derive *analytical lower and upper bounds* on the targets' and vehicles' position uncertainty by exploiting the monotonicity property of the Riccati differential equation arising from the Kalman–Bucy filter. These bounds allow us to study the impact of the sensors' accuracy and the targets' dynamics on the performance of our coordination strategy. Extensive simulation experiments illustrate the proposed theoretical results.

Index Terms—Active sensing, cooperative localization, Kalman filtering, mobile sensors, target tracking, unmanned aerial vehicles.

I. INTRODUCTION

A. Problem Statement and Related Work

THIS paper deals with the deployment of a team of unmanned aerial vehicles in the 3-D space, in order to maximize the accuracy of the position estimate of one or multiple moving targets (*active target-tracking problem*). This problem has relevant applications in surveillance, patrolling, military, and environmental monitoring tasks, and offers different levels of complexity depending on whether the position of the agents is perfectly known or needs to be estimated together with that of the targets (*localization problem*), and on whether a collaborative or a noncooperative approach is adopted. Since testing on real flying platforms is complex,

expensive, and time-consuming, analytical tools are needed to predict the performance of a newly-synthesized algorithm in an early design stage. This paper moves toward this direction and presents analytical results elucidating the role played by the targets' dynamics and the accuracy of the on-board range-finding sensors on the (steady-state) target-tracking and vehicle localization performances.

Multiagent systems research has recently gained a prominent role in the robotics and control literature [1]–[3]. The surge of interest in this subject has been mainly driven by the sheer increase in autonomy, computing power, and sensing of today's robots. An essential capability that each autonomous robot should possess is that of being able to efficiently measure the surrounding environment and to promptly respond to stimuli coming from other robots, humans, or moving targets. Extensive research has been done in the literature on the subject of tracking targets with *static sensors* [4], [5], or on the optimal placement of fixed sensors [6]. *Mobile sensor networks* are known to offer distinctive advantages over static sensor arrays in terms of quality of sensing and estimation, area coverage, adaptability to changing conditions (in the environment as well as in the target's behavior), and robustness against failures. *Cooperative active sensing* leverages the mobility of a robotic sensor network in order to enhance the target tracking performances [7]–[18]; in the simplest instance of this problem, n sensors have to fuse their local measurements and move in order to attain the best position estimate of a moving target. This mechanism is sometimes referred to as "information-driven mobility" in the literature, and it amounts, in practice, to minimize a certain scalar function of the covariance matrix of the position estimates. In *optimum experimental design theory* [6], [19], this function is typically the determinant or the trace of the covariance matrix (D- and A-optimality criteria). In the cooperative active target-tracking literature, a large body of research has focused on agents equipped with sensors providing *range-only* or *range-bearing* measurements to the target, while relatively fewer works have dealt with the more challenging bearing-only case (cf. [20]). Moreover, most of the existing papers have limited themselves to *single targets* moving in a *2-D environment*, and none of them has conducted an *analytical study* of the impact of the system's parameters on the performance of the proposed coordination strategies.

In [7], a motion-planning algorithm has been presented for solving the cooperative 2-D target-tracking problem using range-bearing measurements. The control law proposed by Chung *et al.* [7] is based on the gradient of the determinant of the covariance matrix of the target's position estimate with

F. Morbidi was with the Department of Computer Science and Engineering, University of Texas at Arlington, Arlington, TX 76019 USA. He is now with the Institute for Design and Control of Mechatronical Systems, Johannes Kepler University, Linz 4040, Austria (e-mail: fabio.morbidi@jku.at).

G. L. Mariottini is with the Department of Computer Science and Engineering, University of Texas at Arlington, Arlington, TX 76019 USA (e-mail: gianluca@uta.edu).

respect to each of the robot's coordinates. The multiple-target case is briefly treated as a possible extension, and the role of imperfect communication between agents is also investigated, thus elucidating the trade-offs in performance between sensing and communication. The results in [7] have been extended in two directions in [8]. First, by using dynamic average consensus estimators, the controller proposed in [7] is made distributedly implementable. Second, a new control design procedure based on the distributed Kalman filter [21] for estimation fusion is presented, and the case of range-only sensors is addressed. Pursuing this line of research, the same authors have lately proposed estimation algorithms alternative to the Kalman filter (H$_\infty$ filters, set-valued estimators), and studied the impact of "intelligent" evasive targets on the tracking performances. Embracing an approach similar to [8], the collaborative active-sensing problem has been studied in [9] for a group of double-integrator *ground robots* equipped with range-bearing sensors. The network-connectivity issue is addressed using a flocking-based mobility model (which also accounts for collision avoidance), and a modified version of the distributed Kalman filter in [21] for estimating the target's state is presented, along with information-driven decentralized control laws for the agents. Recently, in [10], a formal closed-loop stability analysis of an enhanced version of the coupled estimation-and-control algorithm described in [9], has been proposed by the same author. However, both in [9] and [10], only the single-target case is addressed. In [11], the authors focused on discrete-time target-tracking for a team of *unicycle robots* with bounds on the positive forward velocity, and showed that the associated optimization problem is NP-hard in general. Nontrivial relaxations to this problem are then proposed for determining the set of feasible locations that each robot should move to, in order to collect the most informative distance measurements. Note that differently from [7], where the nonlinearities inherent to the range-bearing model are "absorbed" into the nonstationary sensor noise, the approach in [11] takes the nonlinear nature of the distance-only measurements explicitly into account. Recently, in [12], the results in [11] have been extended to the case of ground vehicles processing mixtures of relative measurements (i.e., range and/or bearing), and a closed-form global optimal solution for the active-sensing problem is derived in the case of a *single vehicle* for arbitrary target-motion models. In addition, constraints on the maximum speed of the robots and on the minimum distance between the agents and the target have been incorporated into the problem formulation. However, the mathematical tools used in [11] and [12] appear much more involved than those in [7], thus making their approach difficult to extend to different scenarios or to implement in a distributed fashion. Moreover, differently from [7]–[9], inter-agent *cooperation* does not seem fully exploited in [11] and [12]. In [13], an *approximate* tracking algorithm is proposed, where the agents try to minimize the target's location uncertainty using range-bearing sensors. The optimization problem (minimize the determinant of the target-position estimates' covariance matrix), is solved separately by each agent by a greedy search over the discretized set of candidate headings. In [14], the authors studied the optimal placement of range-only sensors

for nonrandom *static-target* position estimation. In this specific scenario, the determinant of the Fisher information matrix (the inverse of the covariance matrix) can be computed in closed-form and its critical points can be easily characterized. An optimal configuration, then turns out to be one in which the sensors are uniformly placed in a circular fashion around the target.

Other related work on cooperative active target tracking has been done in [22], where *constant-speed unicycle robots* are controlled using a distributed behavior-based approach, the communication takes place on a broadcast network and estimation is achieved by an unscented Kalman filter. However, differently from [11], [12], and [14], this paper does not provide a precise theoretical characterization of the properties of the proposed coordination algorithm. Finally, in [23], the authors have studied the optimal routing of two camera-equipped fixed-wing aircraft cruising at *fixed altitude*, cooperatively tracking a single ground target. A perspective transformation relating the image-plane measurements to the ground allows to derive the geolocation error covariance matrix, and dynamic programming is used by the authors to compute optimal coordinated control policies that minimize the fused target localization error covariance.

Besides [7], [8] above, another source of inspiration, for this paper, came from some recent works in the *cooperative localization* literature [24]–[29]. In [24] and [25], the authors used the properties of the Riccati recursion arising from the extended Kalman filter to determine explicit upper bounds for the steady-state accuracy of the *cooperative localization* (CL) and *cooperative simultaneous localization and mapping* (C-SLAM) problems. The analysis in [24] and [25] has been repeated in [26] for the *cooperative localization and target tracking* (CLATT) problem, and it has been shown that robots' localization accuracy improves if the position of multiple moving targets is measured.

B. Original Contributions and Organization

This paper elaborates upon [7], [8] and extends them in several new directions.

First, by using a spherical coordinates representation, we present a generalization for a team of *unmanned aerial vehicles* modeled as double integrators and equipped with 3-D range-finding sensors.

Second, we introduce a gradient-based control design procedure that encompasses the three major optimum experimental design criteria. Our estimation mechanism leverages two different approaches: a *cooperative* one in which the vehicles' target position measurements and covariance matrices of the measurement noise are fused together, and a *noncooperative* approach that relies on tools of dynamic noncooperative game theory. In the first scenario, a Kalman filter is used for the fusion process, while in the second scenario the individual target's position estimates are produced by coupled Kalman filter-like equations.

Third, in the case that the position of the vehicles is *not* perfectly known, we introduce a new problem, termed *active cooperative localization and multitarget tracking* (ACLMT).

In this problem, the aerial vehicles (modeled here as first-order systems) move in the 3-D space along paths that maximize both the accuracy of their *own position estimate* and that of *multiple moving targets*. Taking inspiration from [25] and [26], *analytical lower and upper bounds* on the targets' and vehicles' positioning uncertainty are derived for ACLMT by exploiting the monotonicity property of the Riccati differential equation arising from the Kalman–Bucy filter. These bounds are attractive since they allow us to study the impact of sensors' accuracy and targets' dynamics on the performance of our coordination strategy. Note that the active-sensing problem's formulation considered in [11] and [12] does not lend itself to the insightful performance analysis conducted in this paper, and that ACLMT is, in several respects, more challenging than C-SLAM and CLATT. In fact, the targets' motion in [26] is governed by a simple zero-velocity model (a random walk), and the ground robots in [24]–[26] move in open loop (i.e., there is no control feedback).

It is also worth emphasizing herein that in this paper, we are not specifically concerned with the problem of designing *distributed control laws* for the aerial vehicles. In fact, one can straightforwardly move in this direction, by adapting the distributed strategies proposed in [8] and [9] to our specific setting. Moreover, in order to keep our presentation accessible and concise, we decided not to incorporate *collision-avoidance* or *maximum-speed constraints* in our problem formulation. These issues will be addressed in future, more experiment-oriented works.

This article is based, in part, on previous material presented in [30], compared to which, we provide herein a more comprehensive literature review, new theoretical results and a more extensive numerical validation.

The rest of this paper is organized as follows. Section II presents the measurement model and estimation-and-control strategies for the aerial vehicles, both in the cooperative and noncooperative scenarios. In Section III, the ACLMT problem is introduced, and in Section IV the performance of ACLMT is studied. Finally, in Section V the results of extensive simulation experiments are discussed, and in Section VI, the main contributions of this paper are summarized and possible avenues for future research are outlined.

II. ACTIVE TARGET TRACKING

A. Measurement Model

Consider a team of n aerial vehicles (hereafter, also simply "agents") with positions $\mathbf{p}_1, \ldots, \mathbf{p}_n \in \mathbf{R}^3$ expressed with respect to a common global reference frame, and a target moving in 3-D according to the following model:

$$\dot{\mathbf{x}}(t) = \mathbf{F}\,\mathbf{x}(t) + \mathbf{G}\,\mathbf{u}_{\mathrm{T}}(t) + \mathbf{w}(t) \tag{1}$$

where $\mathbf{x}(t) \in \mathbf{R}^3$ denotes the position of the target at time t, $\mathbf{u}_{\mathrm{T}}(t) \in \mathbf{R}^3$ is an exogenous input, and $\mathbf{w}(t) \in \mathbf{R}^3$ is a continuous-time white Gaussian noise with zero mean and covariance matrix $\mathbf{Q} \in \mathbf{R}^{3 \times 3}$. The observation $\mathbf{z}_i(t) \in \mathbf{R}^3$ of the target's position made by the ith vehicle at time t, is assumed to be given by the following measurement model:

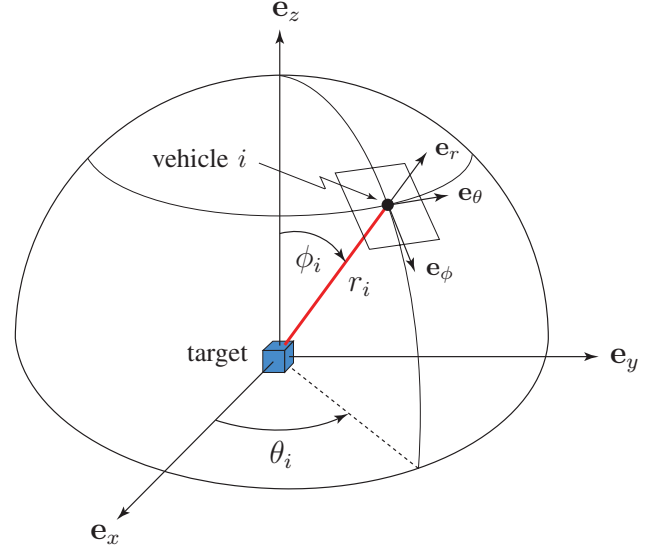$$\mathbf{z}_i(t) = \mathbf{H}_i\,\mathbf{x}(t) + \mathbf{v}_i(t)$$

Fig. 1.   Measurement model for the 3-D range-finding sensor of vehicle i. The spherical coordinates (r_i, θ_i, ϕ_i) have been used, where $r_i \in (0, +\infty)$ is the *distance* from vehicle i to the target, $\theta_i \in (0, 2\pi) \backslash \{\pi\}$ is the *bearing angle* and $\phi_i \in (0, \pi)$ is the *polar angle*. $\{\mathbf{e}_x, \mathbf{e}_y, \mathbf{e}_z\}$, $\{\mathbf{e}_\phi, \mathbf{e}_\theta, \mathbf{e}_r\}$ represent the Cartesian and spherical orthonormal bases, respectively.

where $\mathbf{v}_i(t)$ is a continuous-time zero-mean white Gaussian noise. In the following, we will assume that the measurement noises of the vehicles are independent and that the position $\mathbf{p}_i$ of vehicle i is perfectly known, e.g., from accurate GPS measurements (this last assumption will be relaxed in Section III). In addition, we will suppose that each agent is equipped with a magnetic compass (or an equivalent sensor), which provides its absolute orientation with respect to the fixed global reference frame: in this way, without loss of generality, we can assume that the reference frames attached to the vehicles are all aligned.

By adopting a standard 3-D range-finding sensor model [31, Sec. 4.3.2], we have that $\mathbf{H}_i = \mathbf{I}_3$ (the 3×3 identity matrix) and that the covariance matrix $\mathbf{R}_i^{\mathrm{Car}}(t) \in \mathbf{R}^{3 \times 3}$ of $\mathbf{v}_i(t) \in \mathbf{R}^3$ assumes the form

$$\mathbf{R}_i^{\mathrm{Car}}(t) \triangleq \mathbf{T}_i(t)\,\mathbf{R}_i(t)\,\mathbf{T}_i^T(t) \tag{2}$$

where the rotation matrix $\mathbf{T}_i$ (dropping the time index t), is given by

$$\mathbf{T}_i = \mathcal{R}_z(\theta_i)\mathcal{R}_y(\phi_i) = \begin{bmatrix} \cos\theta_i \cos\phi_i & -\sin\theta_i & \cos\theta_i \sin\phi_i \\ \sin\theta_i \cos\phi_i & \cos\theta_i & \sin\theta_i \sin\phi_i \\ -\sin\phi_i & 0 & \cos\phi_i \end{bmatrix} \tag{3}$$

and $\mathcal{R}_z(\theta_i)$, $\mathcal{R}_y(\phi_i)$ denote the basic 3×3 rotation matrices about the $z-$ and y-axes of an angle θ_i and ϕ_i, respectively (see Fig. 1). $\mathbf{R}_i$ in (2) is the covariance matrix of the measurement noise in the range-bearing-polar frame of vehicle i, and it has the following diagonal structure:

$$\mathbf{R}_i = \mathrm{diag}\!\left(\sigma_{\phi_i}^2, \sigma_{\theta_i}^2, \sigma_{r_i}^2\right). \tag{4}$$

The variance of the range-measurement noise $\sigma_{r_i}^2$ is typically represented by a function $f_r(r_i)$ of the Euclidean distance $r_i \triangleq \|\mathbf{p}_i - \mathbf{x}\|_2$ from agent i to the target [7]; the polar and
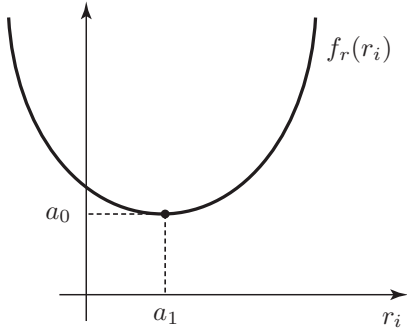
Fig. 2. Uncertainty in measurements is minimal at a distance a_1 from the target. The locus of points at distance a_1 from the target is called the "*sweet spot*" (cf. [7]).

bearing measurement-noise variances $\sigma_{\phi_i}^2$ and $\sigma_{\theta_i}^2$ can also be modeled as dependent on the range r_i through the functions $f_\phi(r_i)$ and $f_\theta(r_i)$, respectively. In this paper, we will consider the following simple form for these functions:

$$
\begin{aligned}
f_r(r_i) &\triangleq a_2(r_i - a_1)^2 + a_0 \\
f_\theta(r_i) &\triangleq \alpha_\theta \, f_r(r_i) \\
f_\phi(r_i) &\triangleq \alpha_\phi \, f_r(r_i)
\end{aligned}
$$

where a_0, a_1, a_2, α_θ, and α_ϕ are strictly positive parameters (however, note that our subsequent results can be straightforwardly extended to the case of general differentiable positive-valued convex functions $f_r(r_i)$, $f_\theta(r_i)$, $f_\phi(r_i)$). This model assumes the existence of a "*sweet spot*" located at a distance a_1 from the target, where uncertainty in measurements is minimal (see Fig. 2). Parameter a_1 depends on the physics of the sensing device, and it may vary from several tens of centimeters for infrared sensors, to few meters for time-of-flight sensors (e.g., ultrasonic sensors). Although environmental factors, such as temperature, humidity, or background noise, might affect the sweet spot, a_1 is typically assumed to be a constant parameter in the literature. It is finally worth observing that a_1, together with the other parameters a_0, a_2, α_θ, and α_ϕ, can be estimated from real data collected by the range-finding sensor, using, for example, standard least-squares methods (cf. [32]).

Remark 1: Note that the transformation (2) from spherical coordinates $\mathbf{R}_i$, to Cartesian coordinates[1] $\mathbf{R}_i^{\mathrm{Car}}$, is valid only for small θ_i and ϕ_i (cf. [4, Sec. 10.4.3]). However, extensive simulation experiments (see Section V), have shown that a violation of this "small-angle condition," does not lead to a significant performance degradation of the target-tracking algorithms proposed in this paper.

In Sections II-B and II-C, we will present a *cooperative* estimation-and-control strategy. In Section II-D, instead, we will describe a *noncooperative* approach that leverages notions of differential game theory, and that is of value in throwing further light on the active target-tracking problem.

---

[1]The spherical coordinates (r, θ, ϕ) are related to the Cartesian coordinates (x, y, z) by the *nonlinear transformation* $r = \sqrt{x^2 + y^2 + z^2}$, $\theta = \mathrm{atan2}(y, x)$, $\phi = \arccos(z/r)$, where $\mathrm{atan2}(\cdot, \cdot)$ stands for the four-quadrant inverse tangent.

B. Cooperative Control

The target-position measurements $\mathbf{z}_i$ and covariances $\mathbf{R}_i^{\mathrm{Car}}$ from the n agents will be fused together to obtain a global target position estimate $\widehat{\mathbf{x}}_{\mathrm{fus}}$ and global position-error covariance $\mathbf{P}_{\mathrm{fus}}$ (see Section II-C). In this section, we will present a cooperative control strategy that moves the aerial vehicles in order to minimize a scalar function of the covariance $\mathbf{P}_{\mathrm{fus}}$, thus reducing the target's localization error (cf. [8]).

In order to show the generality of our approach, for the design of the gradient-based control laws we will simultaneously consider the cost functions for the three most popular optimum experimental design criteria [6, Sec. 2.3]

$$ J = \ln \det(\mathbf{P}_{\mathrm{fus}}) \tag{5} $$

for the D-*optimality* (determinant) criterion

$$ J = \mathrm{tr}(\mathbf{P}_{\mathrm{fus}}) \tag{6} $$

for the A-*optimality* (trace) criterion, and

$$ J = \lambda_{\max}(\mathbf{P}_{\mathrm{fus}}) = \|\mathbf{P}_{\mathrm{fus}}\|_2 \tag{7} $$

for the E-*optimality* criterion, where $\lambda_{\max}(\mathbf{P}_{\mathrm{fus}})$ denotes the maximum eigenvalue of $\mathbf{P}_{\mathrm{fus}}$ and $\|\mathbf{P}_{\mathrm{fus}}\|_2$ is the spectral norm of $\mathbf{P}_{\mathrm{fus}}$. The D-optimum design (the most widely used criterion), minimizes the volume of the uncertainty ellipsoid for the estimates, the E-optimum design minimizes the length of the largest axis of the same ellipsoid, and the A-optimum design suppresses the average variance of the estimates. Note that although the cost functions (5)–(7) are convex with respect to $\mathbf{P}_{\mathrm{fus}}^{-1}$ [assuming that $\mathrm{tr}(\mathbf{P}_{\mathrm{fus}}) = \infty$ and $\lambda_{\max}(\mathbf{P}_{\mathrm{fus}}) = \infty$, if $\det(\mathbf{P}_{\mathrm{fus}}^{-1}) = 0$ (cf. [6, Sec. B.5])], they are *not* convex with respect to the relative position and orientation of the vehicles and target, and they are thus prone to local minima [33].

Since the cost function (7) is *not differentiable* in general (in fact, the gradient of $\lambda_{\max}(\mathbf{P}_{\mathrm{fus}})$ does not exist when the maximum eigenvalue of $\mathbf{P}_{\mathrm{fus}}$ is not simple), in the following, we will consider its *smoothed version* [34]:

$$ \Phi_\varepsilon(\mathbf{P}_{\mathrm{fus}}) = \varepsilon \ln \left(\sum_{i=1}^{3} \exp\big(\lambda_i(\mathbf{P}_{\mathrm{fus}})/\varepsilon\big) \right) $$

where $\varepsilon > 0$ is an assigned smoothing parameter and $\lambda_i(\mathbf{P}_{\mathrm{fus}})$ denotes the ith eigenvalue of $\mathbf{P}_{\mathrm{fus}}$. Note that function $\Phi_\varepsilon(\mathbf{P}_{\mathrm{fus}})$ is of class $\mathcal{C}^\infty$ and it possesses the following uniform approximation property to $\lambda_{\max}(\mathbf{P}_{\mathrm{fus}})$:

$$ 0 \leq \Phi_\varepsilon(\mathbf{P}_{\mathrm{fus}}) - \lambda_{\max}(\mathbf{P}_{\mathrm{fus}}) \leq \varepsilon \ln(3), \qquad \forall \varepsilon > 0 $$

from which it follows that $\lim_{\varepsilon \downarrow 0} \Phi_\varepsilon(\mathbf{P}_{\mathrm{fus}}) = \lambda_{\max}(\mathbf{P}_{\mathrm{fus}})$. As indicated in [35, p. 249], it turns out that when $\varepsilon \in [10^{-4}, 10^{-6}]$, $\Phi_\varepsilon(\mathbf{P}_{\mathrm{fus}})$ yields an excellent approximation to $\lambda_{\max}(\mathbf{P}_{\mathrm{fus}})$.

With the exception of Sections III and IV, the following double-integrator model will be used for the aerial vehicles:

$$
\begin{aligned}
\dot{\mathbf{p}}_i &= \mathbf{q}_i \\
\dot{\mathbf{q}}_i &= \mathbf{u}_i, \qquad i \in \{1, \ldots, n\}
\end{aligned}
\tag{8}
$$

where $\mathbf{q}_i \in \mathbb{R}^3$ denotes the velocity of vehicle i and $\mathbf{u}_i \in \mathbb{R}^3$ its control input. The gradient controller of vehicle i will then be of the form

$$\mathbf{u}_i = -\mathbf{B}\,\mathbf{q}_i - \mathbf{\Gamma}\,\mathbf{T}_i \left[\frac{1}{r_i\,\sin\theta_i}\,\frac{\partial J}{\partial\phi_i},\; \frac{1}{r_i}\,\frac{\partial J}{\partial\theta_i},\; \frac{\partial J}{\partial r_i} \right]^T \quad (9)$$

where $\mathbf{B} \in \mathbb{R}^{3\times3}$, $\mathbf{B} \succ \mathbf{0}$, is a damping matrix and $\mathbf{\Gamma} \in \mathbb{R}^{3\times3}$, $\mathbf{\Gamma} \succ \mathbf{0}$, is a gain matrix[2]. In order to simplify the forthcoming derivations, let us introduce the following 3×3 matrices, whose explicit expression will be given in Section II-C:

$$\mathbf{P}_i^r \triangleq \frac{\partial \mathbf{P}_{\text{fus}}}{\partial r_i}, \quad \mathbf{P}_i^\theta \triangleq \frac{\partial \mathbf{P}_{\text{fus}}}{\partial \theta_i}, \quad \mathbf{P}_i^\phi \triangleq \frac{\partial \mathbf{P}_{\text{fus}}}{\partial \phi_i}. \quad (10)$$

By using [6, Th. B.17], we can explicitly compute the partial derivatives appearing on the right-hand side of (9) for the D-optimality criterion

$$\frac{\partial J}{\partial r_i} = \text{tr}(\mathbf{P}_{\text{fus}}^{-1}\mathbf{P}_i^r), \quad \frac{\partial J}{\partial \theta_i} = \text{tr}(\mathbf{P}_{\text{fus}}^{-1}\mathbf{P}_i^\theta), \quad \frac{\partial J}{\partial \phi_i} = \text{tr}(\mathbf{P}_{\text{fus}}^{-1}\mathbf{P}_i^\phi)$$

for the A-optimality criterion

$$\frac{\partial J}{\partial r_i} = \text{tr}(\mathbf{P}_i^r), \quad \frac{\partial J}{\partial \theta_i} = \text{tr}(\mathbf{P}_i^\theta), \quad \frac{\partial J}{\partial \phi_i} = \text{tr}(\mathbf{P}_i^\phi)$$

and for the E-optimality criterion

$$\frac{\partial J}{\partial r_i} = \text{tr}\big(\mathbf{U}^T\text{diag}(\nabla_\lambda\,\Phi_\varepsilon(\mathbf{P}_{\text{fus}}))\,\mathbf{U}\,\mathbf{P}_i^r\big)$$

$$\frac{\partial J}{\partial \theta_i} = \text{tr}\big(\mathbf{U}^T\text{diag}(\nabla_\lambda\,\Phi_\varepsilon(\mathbf{P}_{\text{fus}}))\,\mathbf{U}\,\mathbf{P}_i^\theta\big)$$

$$\frac{\partial J}{\partial \phi_i} = \text{tr}\big(\mathbf{U}^T\text{diag}(\nabla_\lambda\,\Phi_\varepsilon(\mathbf{P}_{\text{fus}}))\,\mathbf{U}\,\mathbf{P}_i^\phi\big). \quad (11)$$

The lth component of the gradient vector $\nabla_\lambda\,\Phi_\varepsilon(\mathbf{P}_{\text{fus}})$ in (11) is

$$[\nabla_\lambda\,\Phi_\varepsilon(\mathbf{P}_{\text{fus}})]_l = \frac{\exp\big(\lambda_l(\mathbf{P}_{\text{fus}})/\varepsilon\big)}{\sum_{j=1}^3\,\exp\big(\lambda_j(\mathbf{P}_{\text{fus}})/\varepsilon\big)}, \quad l \in \{1, 2, 3\}$$

and the orthogonal matrix $\mathbf{U}$ satisfies $\mathbf{P}_{\text{fus}} = \mathbf{U}^T\text{diag}(\lambda(\mathbf{P}_{\text{fus}}))\mathbf{U}$, where $\text{diag}(\lambda(\mathbf{P}_{\text{fus}}))$ is a diagonal matrix with the elements of the vector $\lambda(\mathbf{P}_{\text{fus}}) \triangleq [\lambda_1(\mathbf{P}_{\text{fus}}), \lambda_2(\mathbf{P}_{\text{fus}}), \lambda_3(\mathbf{P}_{\text{fus}})]^T$, $\lambda_1(\mathbf{P}_{\text{fus}}) \geq \lambda_2(\mathbf{P}_{\text{fus}}) \geq \lambda_3(\mathbf{P}_{\text{fus}})$, put on its main diagonal.

Remark 2: Note that the controller (9) is *centralized* since $\mathbf{P}_{\text{fus}}$, $\mathbf{P}_i^r$, $\mathbf{P}_i^\theta$, and $\mathbf{P}_i^\phi$ contain information from *all* the agents. However, the control law (9) can be implemented in a distributed fashion by replacing any unavailable global quantity with local estimates, as done, e.g., in [8] and [9].

C. Kalman-Filter Fusion

As anticipated in Section II-B, we describe here a method inspired by [8], to fuse the local target position measurements and error covariance matrices: in this way, we can determine the three matrices in (10), necessary for the implementation of controller (9). The method defines $\widehat{\mathbf{x}}_{\text{fus}}$ and $\mathbf{P}_{\text{fus}}$ by means of a Kalman-Bucy filter [36, Sec. 4.5]

$$\dot{\mathbf{P}}_{\text{fus}} = \mathbf{F}\,\mathbf{P}_{\text{fus}} + \mathbf{P}_{\text{fus}}\,\mathbf{F}^T + \mathbf{Q} - \mathbf{P}_{\text{fus}}\,\mathbf{C}\,\mathbf{P}_{\text{fus}} \quad (12)$$

[2]The symbols "$\succ$," "$\succeq$," denote the matrix inequality in the positive definite and positive semidefinite sense, respectively.

$$\dot{\widehat{\mathbf{x}}}_{\text{fus}} = \mathbf{F}\,\widehat{\mathbf{x}}_{\text{fus}} + \mathbf{G}\,\mathbf{u}_{\text{T}} + \mathbf{P}_{\text{fus}}\,(\mathbf{y} - \mathbf{C}\,\widehat{\mathbf{x}}_{\text{fus}}) \quad (13)$$

where

$$\mathbf{C} \triangleq \sum_{i=1}^n (\mathbf{R}_i^{\text{Car}})^{-1}, \quad \mathbf{y} \triangleq \sum_{i=1}^n (\mathbf{R}_i^{\text{Car}})^{-1}\,\mathbf{z}_i$$

and (12) and (13) are, respectively, initialized with

$$\mathbf{P}_{\text{fus}}(t_0) = \left[\sum_{i=1}^n (\mathbf{R}_i^{\text{Car}}(t_0))^{-1} \right]^{-1} \quad (14)$$

$$\widehat{\mathbf{x}}_{\text{fus}}(t_0) = \mathbf{P}_{\text{fus}}(t_0) \sum_{i=1}^n (\mathbf{R}_i^{\text{Car}}(t_0))^{-1}\,\mathbf{z}_i(t_0) \quad (15)$$

where t_0 denotes the initial time instant. Note that (15) is a weighted least-squares estimate for the position of the target, and that (14) is the covariance matrix of the weighted least-squares estimator. By taking the partial derivatives with respect to r_i, θ_i, and ϕ_i on both sides of the *Riccati differential equation* (RDE) (12), we get the following three Lyapunov differential equations:

$$\dot{\mathbf{P}}_i^r = (\mathbf{F} - \mathbf{P}_{\text{fus}}\,\mathbf{C})\mathbf{P}_i^r + \mathbf{P}_i^r(\mathbf{F} - \mathbf{P}_{\text{fus}}\,\mathbf{C})^T$$
$$+ 2\,a_2(r_i - a_1)\,\mathbf{P}_{\text{fus}}\,\mathbf{T}_i\,\mathbf{R}_i^{-2}\,\text{diag}(\alpha_\phi,\,\alpha_\theta,\,1)\,\mathbf{T}_i^T\,\mathbf{P}_{\text{fus}}$$

$$\dot{\mathbf{P}}_i^\theta = (\mathbf{F} - \mathbf{P}_{\text{fus}}\,\mathbf{C})\mathbf{P}_i^\theta + \mathbf{P}_i^\theta(\mathbf{F} - \mathbf{P}_{\text{fus}}\,\mathbf{C})^T$$
$$- \mathbf{P}_{\text{fus}}(\mathbf{A}_{\theta_i} + \mathbf{A}_{\theta_i}^T)\mathbf{P}_{\text{fus}}, \quad \mathbf{A}_{\theta_i} = \mathbf{\Theta}\,\mathbf{T}_i\,\mathbf{R}_i^{-1}\,\mathbf{T}_i^T$$

$$\dot{\mathbf{P}}_i^\phi = (\mathbf{F} - \mathbf{P}_{\text{fus}}\,\mathbf{C})\mathbf{P}_i^\phi + \mathbf{P}_i^\phi(\mathbf{F} - \mathbf{P}_{\text{fus}}\,\mathbf{C})^T$$
$$- \mathbf{P}_{\text{fus}}(\mathbf{A}_{\phi_i} + \mathbf{A}_{\phi_i}^T)\mathbf{P}_{\text{fus}}, \quad \mathbf{A}_{\phi_i} = \mathbf{T}_i\,\mathbf{\Upsilon}\,\mathbf{R}_i^{-1}\,\mathbf{T}_i^T \quad (16)$$

where

$$\mathbf{\Theta} = \begin{bmatrix} 0 & -1 & 0 \\ 1 & 0 & 0 \\ 0 & 0 & 0 \end{bmatrix}, \quad \mathbf{\Upsilon} = \begin{bmatrix} 0 & 0 & 1 \\ 0 & 0 & 0 \\ -1 & 0 & 0 \end{bmatrix}.$$

The equations in (16) are respectively initialized with

$$\mathbf{P}_i^r(t_0) = 2\,a_2(r_i(t_0) - a_1)\,\mathbf{P}_{\text{fus}}(t_0)\,\mathbf{T}_i(t_0)\,\mathbf{R}_i^{-2}(t_0) \cdot$$
$$\text{diag}(\alpha_\phi, \alpha_\theta, 1)\,\mathbf{T}_i^T(t_0)\,\mathbf{P}_{\text{fus}}(t_0)$$
$$\mathbf{P}_i^\theta(t_0) = -\mathbf{P}_{\text{fus}}(t_0)\big(\mathbf{A}_{\theta_i}(t_0) + \mathbf{A}_{\theta_i}^T(t_0)\big)\mathbf{P}_{\text{fus}}(t_0)$$
$$\mathbf{P}_i^\phi(t_0) = -\mathbf{P}_{\text{fus}}(t_0)\big(\mathbf{A}_{\phi_i}(t_0) + \mathbf{A}_{\phi_i}^T(t_0)\big)\mathbf{P}_{\text{fus}}(t_0).$$

D. Noncooperative Estimation and Control

In Sections II-B and II-C, we have assumed that the n aerial vehicles coordinate their 3-D motion in order to estimate the position of the target as accurately as possible. In this section, we briefly explore the converse scenario (of potential interest, e.g., in a military setting) in which antagonistic agents *compete* with each other in order to optimally estimate the location of the moving target. The control strategy obtained in this case is more amenable to a decentralized implementation than that presented in Section II-B, but as it is natural to expect, it leads to less accurate individual estimates of the target's position (cf. Figs. 4 and 5). More specifically, in this section we re-interpret the active-target tracking problem as an n-person noncooperative nonzero-sum differential game [37, Sec. 6.1], and we are interested in the existence of possible *feedback Nash equilibrium strategies* [38]. As shown in Corollary A-1 of [39],

for the class of n-person linear-quadratic differential games, a set of these equilibrium strategies can be expressed in closed-form. The dualization of (A-16) of this corollary (with zero cross-weighting matrices), leads to the following Kalman filter-like equations for $i \in \{1, \ldots, n\}$:

$$\dot{\mathbf{P}}_i = \mathbf{F} \mathbf{P}_i + \mathbf{P}_i \mathbf{F}^T + \mathbf{Q}$$
$$- \sum_{\substack{j=1 \\ j \neq i}}^{n} \mathbf{P}_i ((\mathbf{R}_j^{\mathrm{Car}})^{-1} \mathbf{P}_j) - \sum_{j=1}^{n} ((\mathbf{R}_j^{\mathrm{Car}})^{-1} \mathbf{P}_j)^T \mathbf{P}_i \quad (17)$$

$$\dot{\hat{\mathbf{x}}}_i = \mathbf{F} \hat{\mathbf{x}}_i + \mathbf{G} \mathbf{u}_{\mathrm{T}} + \mathbf{P}_i (\mathbf{R}_i^{\mathrm{Car}})^{-1} (\mathbf{z}_i - \hat{\mathbf{x}}_i) \quad (18)$$

where (17) are n coupled RDEs, and $\hat{\mathbf{x}}_i$ and $\mathbf{P}_i$ denote the target's position estimate of agent i and the associated error covariance matrix, respectively. Similarly to Section II-C, we can initialize (17) and (18) with $\mathbf{P}_i(t_0) = \mathbf{R}_i^{\mathrm{Car}}(t_0)$ and $\hat{\mathbf{x}}_i(t_0) = \mathbf{P}_i(t_0) (\mathbf{R}_i^{\mathrm{Car}}(t_0))^{-1} \mathbf{z}_i(t_0)$, respectively. Note that Lemma 6.6.1 of [37], ensures the existence of positive-semidefinite solutions to (17).

In the noncooperative framework described in this section, we can define the gradient controller for agent i as

$$\mathbf{u}_i = -\mathbf{B} \mathbf{q}_i - \mathbf{\Gamma} \mathbf{T}_i \left[\frac{1}{r_i \sin \theta_i} \frac{\partial J_i}{\partial \phi_i}, \frac{1}{r_i} \frac{\partial J_i}{\partial \theta_i}, \frac{\partial J_i}{\partial r_i} \right]^T \quad (19)$$

where $J_i = \ln \det(\mathbf{P}_i)$, or alternatively $J_i = \mathrm{tr}(\mathbf{P}_i)$, $J_i = \lambda_{\max}(\mathbf{P}_i)$ [cf. (9)]. In order to write concise equations in the remaining of this section, let us introduce (with a slight abuse of notation), the following 3×3 matrices for all $i, k \in \{1, \ldots, n\}$:

$$\mathbf{P}_{ik}^r \triangleq \frac{\partial \mathbf{P}_i}{\partial r_k}, \quad \mathbf{P}_{ik}^\theta \triangleq \frac{\partial \mathbf{P}_i}{\partial \theta_k}, \quad \mathbf{P}_{ik}^\phi \triangleq \frac{\partial \mathbf{P}_i}{\partial \phi_k}.$$

By using [6, Th. B.17], we can compute, as before, the partial derivatives appearing on the right-hand side of (19), for the D-, A-, and E-optimality criteria. For the sake of brevity, we only report here the explicit expressions for the first criterion

$$\frac{\partial J_i}{\partial r_i} = \mathrm{tr}(\mathbf{P}_i^{-1} \mathbf{P}_{ii}^r), \quad \frac{\partial J_i}{\partial \theta_i} = \mathrm{tr}(\mathbf{P}_i^{-1} \mathbf{P}_{ii}^\theta), \quad \frac{\partial J_i}{\partial \phi_i} = \mathrm{tr}(\mathbf{P}_i^{-1} \mathbf{P}_{ii}^\phi) \quad (20)$$

being the others easily deducible from the equations in Section II-B. The matrix $\mathbf{P}_{ii}^r$ in (20), is obtained by integrating the following n^2 coupled Lyapunov differential equations for $i, k \in \{1, \ldots, n\}$:

$$\dot{\mathbf{P}}_{ik}^r = \mathbf{E} \mathbf{P}_{ik}^r + \mathbf{P}_{ik}^r \mathbf{E}^T - \sum_{\substack{j=1 \\ j \neq i}}^{n} (\mathbf{W}_{ij} \mathbf{P}_{jk}^r + \mathbf{P}_{jk}^r \mathbf{W}_{ij}^T) - \mathbf{\Omega}_{ik} \quad (21)$$

where

$$\mathbf{E} \triangleq \mathbf{F} - \sum_{j=1}^{n} \mathbf{P}_j (\mathbf{R}_j^{\mathrm{Car}})^{-1}, \quad \mathbf{W}_{ij} \triangleq \mathbf{P}_i (\mathbf{R}_j^{\mathrm{Car}})^{-1}$$

$$\mathbf{\Omega}_{ik} \triangleq \rho_{ik} \left[\mathbf{P}_i \frac{\partial (\mathbf{R}_k^{\mathrm{Car}})^{-1}}{\partial r_k} \mathbf{P}_k + \mathbf{P}_k \frac{\partial (\mathbf{R}_k^{\mathrm{Car}})^{-1}}{\partial r_k} \mathbf{P}_i \right]$$

$$\frac{\partial (\mathbf{R}_k^{\mathrm{Car}})^{-1}}{\partial r_k} = -2 a_2 (r_k - a_1) \mathbf{T}_k \mathbf{R}_k^{-2} \mathrm{diag}(\alpha_\phi, \alpha_\theta, 1) \mathbf{T}_k^T$$

with $\rho_{ik} = 1/2$ if $i = k$, and $\rho_{ik} = 1$ otherwise. Analogously, $\mathbf{P}_{ii}^\theta$ and $\mathbf{P}_{ii}^\phi$ in (20) are obtained from the integration of the following coupled Lyapunov differential equations for $i, k \in \{1, \ldots, n\}$:

$$\dot{\mathbf{P}}_{ik}^\theta = \mathbf{E} \mathbf{P}_{ik}^\theta + \mathbf{P}_{ik}^\theta \mathbf{E}^T - \sum_{\substack{j=1 \\ j \neq i}}^{n} (\mathbf{W}_{ij} \mathbf{P}_{jk}^\theta + \mathbf{P}_{jk}^\theta \mathbf{W}_{ij}^T)$$
$$- \rho_{ik} [\mathbf{P}_i (\mathbf{A}_{\theta_k} + \mathbf{A}_{\theta_k}^T) \mathbf{P}_k + \mathbf{P}_k (\mathbf{A}_{\theta_k} + \mathbf{A}_{\theta_k}^T) \mathbf{P}_i]$$

$$\dot{\mathbf{P}}_{ik}^\phi = \mathbf{E} \mathbf{P}_{ik}^\phi + \mathbf{P}_{ik}^\phi \mathbf{E}^T - \sum_{\substack{j=1 \\ j \neq i}}^{n} (\mathbf{W}_{ij} \mathbf{P}_{jk}^\phi + \mathbf{P}_{jk}^\phi \mathbf{W}_{ij}^T)$$
$$- \rho_{ik} [\mathbf{P}_i (\mathbf{A}_{\phi_k} + \mathbf{A}_{\phi_k}^T) \mathbf{P}_k + \mathbf{P}_k (\mathbf{A}_{\phi_k} + \mathbf{A}_{\phi_k}^T) \mathbf{P}_i] \quad (22)$$

where $\mathbf{A}_{\theta_k}$ and $\mathbf{A}_{\phi_k}$ are defined as in (16), and (21) and (22) are initialized analogously to the equations in (16).

III. ACTIVE COOPERATIVE LOCALIZATION AND MULTITARGET TRACKING (ACLMT)

In this section, we extend the *cooperative scenario* described in Sections II-B and II-C to one in which we have *m moving targets* with positions $\mathbf{x}_1, \ldots, \mathbf{x}_m$ and n aerial vehicles whose location $\mathbf{p}_1, \ldots, \mathbf{p}_n$ is *not* exactly known. The agents simultaneously perform vehicle-to-target and vehicle-to-vehicle relative measurements, and they move along trajectories that maximize the accuracy of both their own and the other targets' and vehicles' position estimate. We will refer to this new problem as *active cooperative localization and multi-target tracking* (ACLMT). In what follows, we will assume that each vehicle is capable of distinguishing the other agents/targets. The "assignment information" (i.e., *which* vehicle is assigned to *which* vehicle/target) is incorporated into the *association matrix* $\mathbf{\Lambda}$, that, as we will see later in this section, is instrumental in defining the control for the n vehicles.

Definition 1: (Association matrix $\mathbf{\Lambda}$): Let $\mathbf{x}_{\mathrm{tot}} \triangleq [\mathbf{x}_1^T, \ldots, \mathbf{x}_m^T, \mathbf{p}_1^T, \ldots, \mathbf{p}_n^T]^T \in \mathbb{R}^{3(m+n)}$ be the stacked vector of the positions of the m targets and n vehicles. Let $\mathcal{G}(\mathbf{x}_{\mathrm{tot}}(t)) = (\mathcal{V}, \mathcal{T} \cup \mathcal{V}, \mathcal{E}(\mathbf{x}_{\mathrm{tot}}(t)))$ be a bipartite dynamic digraph with vertex sets $\mathcal{V}$ and $\mathcal{T} \cup \mathcal{V}$ ($\mathcal{V} = \{\mathrm{V}_1, \ldots, \mathrm{V}_n\}$ is the set of vehicles and $\mathcal{T} = \{\mathrm{T}_1, \ldots, \mathrm{T}_m\}$ the set of targets), and edge set $\mathcal{E}(\mathbf{x}_{\mathrm{tot}}(t))$ (obviously, $(\mathrm{V}_i, \mathrm{V}_i) \notin \mathcal{E}(\mathbf{x}_{\mathrm{tot}}(t))$, for all i and t). We define the *association matrix* of $\mathcal{G}(\mathbf{x}_{\mathrm{tot}}(t))$ (see the illustrative example in Fig. 3), to be the $n \times (m+n)$ matrix $\mathbf{\Lambda}(\mathbf{x}_{\mathrm{tot}}(t)) = [\ell_{ih}(\mathbf{x}_{\mathrm{tot}}(t))]$, $\sum_{h=1}^{m+n} \ell_{ih}(\mathbf{x}_{\mathrm{tot}}(t)) = 1$, such that $\ell_{ih}(\mathbf{x}_{\mathrm{tot}}(t)) > 0$ if $(\mathrm{V}_i, [\mathcal{T} \cup \mathcal{V}]_h) \in \mathcal{E}(\mathbf{x}_{\mathrm{tot}}(t))$ and $\ell_{ih}(\mathbf{x}_{\mathrm{tot}}(t)) = 0$ otherwise, $i \in \{1, \ldots, n\}$, $h \in \{1, \ldots, m+n\}$, where $[\mathcal{T} \cup \mathcal{V}]_h$ denotes the hth element of the set $\mathcal{T} \cup \mathcal{V}$.

We will assume that $\ell_{ih}(\mathbf{x}_{\mathrm{tot}}(t)) = 0$ when vehicle i is not able to sense the hth target/vehicle at time t. On the other hand, the value of the positive weights $\ell_{ih}(\mathbf{x}_{\mathrm{tot}}(t))$ may vary according to the distance of vehicle i to the hth target/vehicle or it may be chosen according to other priority/hierarchical criteria, depending on the specific application scenario.

By extending (1), let us suppose that the motion of the targets is governed by

$$\dot{\mathbf{x}}_j = \mathbf{F}_j \mathbf{x}_j + \mathbf{G}_j \mathbf{u}_{\mathrm{T}j} + \mathbf{w}_j, \quad j \in \{1, \ldots, m\} \quad (23)$$

$$\Lambda(\mathbf{x}_{\text{tot}}) = \begin{bmatrix} T_1 & T_2 & V_1 & V_2 & V_3 \\ 1/3 & 0 & 0 & 1/3 & 1/3 \\ 1 & 0 & 0 & 0 & 0 \\ 0 & 1/2 & 1/2 & 0 & 0 \end{bmatrix} \begin{matrix} V_1 \\ V_2 \\ V_3 \end{matrix}$$
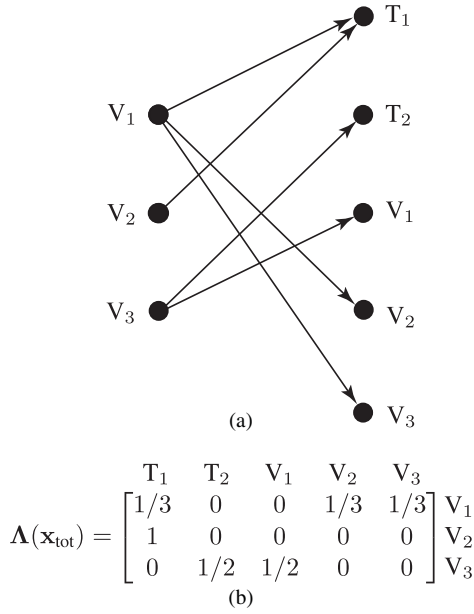
(b)

Fig. 3. *Example of association matrix.* (a) Bipartite digraph $\mathcal{G}(\mathbf{x}_{\text{tot}})$ in the case of three vehicles $\{V_1, V_2, V_3\}$ and two targets $\{T_1, T_2\}$. (b) Corresponding 3×5 association matrix $\Lambda(\mathbf{x}_{\text{tot}})$.

where $\mathbf{x}_j \in \mathbb{R}^3$ is the position of the target j, $\mathbf{u}_{Tj} \in \mathbb{R}^3$ is an exogenous input and $\mathbf{w}_j \in \mathbb{R}^3$ is a continuous-time zero-mean white Gaussian noise with covariance matrix $\mathbf{Q}_j \in \mathbb{R}^{3 \times 3}$.

Differently from the preceding section, we suppose here that the motion of the aerial vehicles is governed by the following first-order model[3]:

$$\dot{\mathbf{p}}_i = \mathbf{u}_i + \mathbf{n}_i, \qquad i \in \{1, \ldots, n\} \qquad (24)$$

where $\mathbf{p}_i \in \mathbb{R}^3$ is the position of agent i, $\mathbf{u}_i \in \mathbb{R}^3$ its control input, and $\mathbf{n}_i \in \mathbb{R}^3$ is a continuous-time white Gaussian noise with zero mean and diagonal covariance matrix $\mathbf{N}_i \in \mathbb{R}^{3 \times 3}$. By combining (23) and (24) together, we obtain the following system:

$$\begin{aligned} \dot{\mathbf{x}}_{\text{tot}} &= \mathbf{F}_{\text{tot}} \mathbf{x}_{\text{tot}} + \mathbf{G}_{\text{tot}} \mathbf{u}_{\text{tot}} + \mathbf{w}_{\text{tot}} \\ &\triangleq \text{blkdiag}\big(\mathbf{F}_1, \ldots, \mathbf{F}_m, \mathbf{0}_{3 \times 3}, \ldots, \mathbf{0}_{3 \times 3}\big) \mathbf{x}_{\text{tot}} \\ &\quad + \text{blkdiag}\big(\mathbf{G}_1, \ldots, \mathbf{G}_m, \mathbf{I}_3, \ldots, \mathbf{I}_3\big) \mathbf{u}_{\text{tot}} + \mathbf{w}_{\text{tot}} \end{aligned} \qquad (25)$$

where $\mathbf{u}_{\text{tot}} \triangleq [\mathbf{u}_{T1}^T, \ldots, \mathbf{u}_{Tm}^T, \mathbf{u}_1^T, \ldots, \mathbf{u}_n^T]^T \in \mathbb{R}^{3(m+n)}$, $\mathbf{w}_{\text{tot}} \triangleq [\mathbf{w}_1^T, \ldots, \mathbf{w}_m^T, \mathbf{n}_1^T, \ldots, \mathbf{n}_n^T]^T \in \mathbb{R}^{3(m+n)}$, blkdiag(·) denotes a block diagonal matrix obtained by the concatenation of its matrix arguments, and $\mathbf{0}_{3 \times 3}$ is the 3×3 matrix of zeros.

As in Section II-A, we assume here that vehicle i is equipped with a 3-D range-finding sensor: this time, however, we will suppose that the position $\mathbf{p}_i$ of agent i is *not* perfectly known. Then the measurement model of agent i will take the form

$$\mathbf{z}_i = \mathbf{x}_{\text{tot}} + \mathbf{v}_i + \mathbf{d}_i, \qquad i \in \{1, \ldots, n\} \qquad (26)$$

---

[3]Note that owing to our 3-D range-finding sensor model [31, Section 4.3.2], the adoption of a second-order model for the vehicles would make the implementation of the Kalman–Bucy filter more problematic. On the other hand, if we set $\mathbf{H}_i = \mathbf{I}_{3(m+2n)}$ instead of $\mathbf{H}_i = [\mathbf{I}_{3(m+n)} \quad \mathbf{0}_{3(m+n) \times 3n}]$, each double-integrator agent should also measure the velocity of its teammates besides their position, which is impractical in a real application.

where the covariance matrix $\mathbf{R}_i^{\text{Car}}$ of the vehicle-to-target/vehicle-to-vehicle measurement noise $\mathbf{v}_i \in \mathbb{R}^{3(m+n)}$ is again of the form (2), but with

$$\mathbf{R}_i = \text{blkdiag}(\mathbf{R}_{T1}^{Vi}, \ldots, \mathbf{R}_{Tm}^{Vi}, \mathbf{R}_{V1}^{Vi}, \ldots, \mathbf{R}_{Vn}^{Vi})$$

and

$$\mathbf{T}_i = \text{blkdiag}(\mathbf{T}_{T1}^{Vi}, \ldots, \mathbf{T}_{Tm}^{Vi}, \mathbf{T}_{V1}^{Vi}, \ldots, \mathbf{T}_{Vn}^{Vi})$$

where $\mathbf{R}_{Tj}^{Vi}$, $\mathbf{R}_{Vk}^{Vi} \in \mathbb{R}^{3 \times 3}$ are covariance matrices of the form (4) and $\mathbf{T}_{Tj}^{Vi}$, $\mathbf{T}_{Vk}^{Vi} \in \mathbb{R}^{3 \times 3}$ are rotation matrices of the form (3), relative to vehicle i with respect to target $j \in \{1, \ldots, m\}$ and vehicle $k \in \{1, \ldots, n\}$, respectively. Note that, in particular, $\mathbf{R}_{Vi}^{Vi} = \mathbf{0}_{3 \times 3}$ and $\mathbf{T}_{Vi}^{Vi} = \mathbf{I}_3$. The zero-mean white Gaussian noise $\mathbf{d}_i \in \mathbb{R}^{3(m+n)}$ models the uncertainty on the self-localization of vehicle i and its covariance matrix is

$$\Delta_i = \text{blkdiag}(\mathbf{D}_i, \ldots, \mathbf{D}_i)$$

where $\mathbf{D}_i$ is a 3×3 diagonal matrix. The noises $\mathbf{v}_i$ and $\mathbf{d}_i$ are assumed to be independent. The fusion method described in Section II-C is still valid in the more challenging scenario studied in this section as long as suitable modifications are introduced. In particular, the equations of the Kalman–Bucy filter for system (25) and (26), are now

$$\dot{\mathbf{P}}_{\text{fus}} = \mathbf{F}_{\text{tot}} \mathbf{P}_{\text{fus}} + \mathbf{P}_{\text{fus}} \mathbf{F}_{\text{tot}}^T + \mathbf{Q}_{\text{tot}} - \mathbf{P}_{\text{fus}} \mathbf{C}_{\text{tot}} \mathbf{P}_{\text{fus}} \qquad (27)$$

$$\dot{\hat{\mathbf{x}}}_{\text{fus}} = \mathbf{F}_{\text{tot}} \hat{\mathbf{x}}_{\text{fus}} + \mathbf{G}_{\text{tot}} \mathbf{u}_{\text{tot}} + \mathbf{P}_{\text{fus}} (\mathbf{y}_{\text{tot}} - \mathbf{C}_{\text{tot}} \hat{\mathbf{x}}_{\text{fus}}) \qquad (28)$$

where

$$\mathbf{C}_{\text{tot}} \triangleq \sum_{i=1}^n (\mathbf{R}_i^{\text{Car}} + \Delta_i)^{-1}$$

$$\mathbf{y}_{\text{tot}} \triangleq \sum_{i=1}^n (\mathbf{R}_i^{\text{Car}} + \Delta_i)^{-1} \mathbf{z}_i$$

$$\mathbf{Q}_{\text{tot}} \triangleq \text{blkdiag}(\mathbf{Q}_1, \ldots, \mathbf{Q}_m, \mathbf{N}_1, \ldots, \mathbf{N}_n).$$

Equations (27) and (28) are initialized with (14) and (15), where $\mathbf{R}_i^{\text{Car}}(t_0)$ is replaced with $\mathbf{R}_i^{\text{Car}}(t_0) + \Delta_i$. Let now $\mathbf{u}_{i|h}$ denote the gradient control of vehicle i due to the influence of the hth vehicle/target

$$\mathbf{u}_{i|h} = -\Gamma \mathbf{T}_{i|h} \left[\frac{1}{r_{i|h} \sin \theta_{i|h}} \frac{\partial J}{\partial \phi_{i|h}}, \frac{1}{r_{i|h}} \frac{\partial J}{\partial \theta_{i|h}}, \frac{\partial J}{\partial r_{i|h}} \right]^T$$

where the symbols $\mathbf{T}_{i|h}$, $r_{i|h}$, $\theta_{i|h}$, and $\phi_{i|h}$ have an obvious meaning [cf. (9) and (24)]. Then, according to Definition 1, we can write the (overall) control $\mathbf{u}_i$ of vehicle i, as (cf. [8])

$$\mathbf{u}_i \triangleq \sum_{h=1}^{m+n} \ell_{ih}(\mathbf{x}_{\text{tot}}) \mathbf{u}_{i|h}, \qquad i \in \{1, \ldots, n\}.$$

IV. PERFORMANCE OF ACLMT

In this section, we will derive *analytical bounds* on the covariance matrix $\mathbf{P}_{\text{fus}}$ of the Kalman–Bucy filter for system (25) and (26), that will allow us to study the role played by the sensors' accuracy and targets' dynamics on the performance of ACLMT.

In order to state the two main results of this section (Propositions 1 and 2), we briefly review here an interesting property of *Hermitian Riccati differential equations* (HRDEs) [37, Ch. 2]. Consider the following RDE:

$$\dot{\mathbf{P}} = -\mathbf{A}^*(t)\mathbf{P} - \mathbf{P}\mathbf{A}(t) - \mathbf{M}(t) + \mathbf{P}\,\mathbf{S}(t)\mathbf{P}, \qquad t \in \mathcal{I} \quad (29)$$

where $\mathbf{A}^*(t)$ is the conjugate transpose of $\mathbf{A}(t) \in \mathbb{C}^{q \times q}$, and $\mathbf{M}(t), \mathbf{S}(t)$ are $q \times q$ Hermitian matrices for $t \in \mathcal{I} \subset \mathbb{R}_{\geq 0}$. The coefficients $\mathbf{A}(t)$, $\mathbf{M}(t)$, and $\mathbf{S}(t)$ are assumed to be piecewise continuous, locally bounded functions of time. Equation (29) is called HRDE since its solutions with Hermitian initial values $\mathbf{P}(t_0)$, are Hermitian.

The following *comparison theorem* [37, Th. 4.1.4], shows that Hermitian solutions of HRDEs are *monotonically* dependent on *initial values* and on the *coefficients*: in other words, the solutions of HRDEs tend to preserve their ordering with respect to positive definiteness as their argument changes.

Theorem 1 (Comparison theorem): Let $\mathcal{I} \subset \mathbb{R}_{\geq 0}$ be some interval, $t_0 \in \mathcal{I}$ and let the Hamiltonian matrices[4]

$$\begin{bmatrix} \mathbf{A}_j(t) & -\mathbf{S}_j(t) \\ -\mathbf{M}_j(t) & -\mathbf{A}_j^*(t) \end{bmatrix}, \qquad j \in \{1, 2\}$$

be piecewise continuous and locally bounded on $\mathcal{I}$, with $\mathbf{S}_j(t)$ and $\mathbf{M}_j(t)$ Hermitian matrices for $t \in \mathcal{I}$. If $\mathbf{P}_j$, $j \in \{1, 2\}$, are on $\mathcal{I}$ solutions of

$$\dot{\mathbf{P}}_j = -\mathbf{A}_j^*(t)\mathbf{P}_j - \mathbf{P}_j\mathbf{A}_j(t) - \mathbf{M}_j(t) + \mathbf{P}_j\mathbf{S}_j(t)\mathbf{P}_j \quad (30)$$

with $\mathbf{P}_1(t_0) \succeq \mathbf{P}_2(t_0)$ and $\mathbf{P}_1(t_0), \mathbf{P}_2(t_0)$ Hermitian, then

$$\begin{bmatrix} \mathbf{M}_1(t) & \mathbf{A}_1^*(t) \\ \mathbf{A}_1(t) & -\mathbf{S}_1(t) \end{bmatrix} \succeq \begin{bmatrix} \mathbf{M}_2(t) & \mathbf{A}_2^*(t) \\ \mathbf{A}_2(t) & -\mathbf{S}_2(t) \end{bmatrix}, \qquad \text{for } t \in \mathcal{I} \quad (31)$$

implies $\mathbf{P}_1(t) \succeq \mathbf{P}_2(t)$ for $t \in \mathcal{I} \cap [t_0, +\infty)$, i.e., the solutions of (30) depend monotonically on

$$\begin{bmatrix} \mathbf{M}_j(t) & \mathbf{A}_j^*(t) \\ \mathbf{A}_j(t) & -\mathbf{S}_j(t) \end{bmatrix}, \qquad j \in \{1, 2\}$$

(and in particular on $\mathbf{M}_j(t)$ and $-\mathbf{S}_j(t)$) and on the initial value $\mathbf{P}_j(t_0)$. ∎

From Theorem I, we immediately deduce the following result concerning the existence of *lower* and *upper bounds* on the solution of the RDE (27).

Proposition 1 (Bounds on $\mathbf{P}_{\text{fus}}$): Let $\mathcal{I} \subset \mathbb{R}_{\geq 0}$ be some interval, and $t_0 \in \mathcal{I}$. If $\mathbf{P}_{\text{fus}}^{\text{L}}$, $\mathbf{P}_{\text{fus}}$, and $\mathbf{P}_{\text{fus}}^{\text{U}}$ are on $\mathcal{I}$ solutions of the following RDEs:

$$\dot{\mathbf{P}}_{\text{fus}}^{\text{L}} = \mathbf{F}_{\text{tot}}\mathbf{P}_{\text{fus}}^{\text{L}} + \mathbf{P}_{\text{fus}}^{\text{L}}\mathbf{F}_{\text{tot}}^T + \mathbf{Q}_{\text{tot}} - \mathbf{P}_{\text{fus}}^{\text{L}}\mathbf{C}_{\text{tot}}^{\text{U}}\mathbf{P}_{\text{fus}}^{\text{L}} \quad (32)$$

$$\dot{\mathbf{P}}_{\text{fus}} = \mathbf{F}_{\text{tot}}\mathbf{P}_{\text{fus}} + \mathbf{P}_{\text{fus}}\mathbf{F}_{\text{tot}}^T + \mathbf{Q}_{\text{tot}} - \mathbf{P}_{\text{fus}}\mathbf{C}_{\text{tot}}(t)\mathbf{P}_{\text{fus}} \quad (33)$$

$$\dot{\mathbf{P}}_{\text{fus}}^{\text{U}} = \mathbf{F}_{\text{tot}}\mathbf{P}_{\text{fus}}^{\text{U}} + \mathbf{P}_{\text{fus}}^{\text{U}}\mathbf{F}_{\text{tot}}^T + \mathbf{Q}_{\text{tot}} - \mathbf{P}_{\text{fus}}^{\text{U}}\mathbf{C}_{\text{tot}}^{\text{L}}\mathbf{P}_{\text{fus}}^{\text{U}} \quad (34)$$

with $\mathbf{P}_{\text{fus}}^{\text{L}}(t_0) = \mathbf{P}_{\text{fus}}(t_0) = \mathbf{P}_{\text{fus}}^{\text{U}}(t_0)$, $\mathbf{P}_{\text{fus}}(t_0)$ symmetric, and $\mathbf{C}_{\text{tot}}^{\text{L}}$, $\mathbf{C}_{\text{tot}}^{\text{U}}$ constant symmetric matrices, then

$$\mathbf{C}_{\text{tot}}^{\text{L}} \preceq \mathbf{C}_{\text{tot}}(t) \preceq \mathbf{C}_{\text{tot}}^{\text{U}}, \qquad \text{for } t \in \mathcal{I}$$

implies

$$\mathbf{P}_{\text{fus}}^{\text{L}}(t) \preceq \mathbf{P}_{\text{fus}}(t) \preceq \mathbf{P}_{\text{fus}}^{\text{U}}(t), \quad \text{for } t \in \mathcal{I} \cap [t_0, +\infty). \quad (35)$$

[4]A matrix $\mathcal{H} \in \mathbb{C}^{2q \times 2q}$ is called *Hamiltonian* if $\mathscr{I}\mathcal{H} = (\mathscr{I}\mathcal{H})^*$, where $\mathscr{I} \triangleq \begin{bmatrix} \mathbf{0} & -\mathbf{I}_q \\ \mathbf{I}_q & \mathbf{0} \end{bmatrix}$ is the unit imaginary matrix [37, Def. 2.1.1 (*iii*)].

Proof: The result can be proved by performing the following substitutions in the statement of Theorem 1 [we consider herein only the first pair of equations (32) and (33); a similar reasoning applies to the second pair (33) and (34)]:

$$\mathbf{P}_1(t) \to \mathbf{P}_{\text{fus}}(t), \qquad \mathbf{P}_2(t) \to \mathbf{P}_{\text{fus}}^{\text{L}}(t)$$
$$-\mathbf{A}_1^*(t), -\mathbf{A}_2^*(t) \to \mathbf{F}_{\text{tot}}, \quad -\mathbf{M}_1(t), -\mathbf{M}_2(t) \to \mathbf{Q}_{\text{tot}}$$
$$-\mathbf{S}_1(t) \to \mathbf{C}_{\text{tot}}^{\text{U}}, \qquad -\mathbf{S}_2(t) \to \mathbf{C}_{\text{tot}}(t).$$

It is easy to verify that the Hamiltonian matrices

$$\begin{bmatrix} -\mathbf{F}_{\text{tot}}^T & \mathbf{C}_{\text{tot}}^{\text{U}} \\ \mathbf{Q}_{\text{tot}} & \mathbf{F}_{\text{tot}} \end{bmatrix}, \quad \begin{bmatrix} -\mathbf{F}_{\text{tot}}^T & \mathbf{C}_{\text{tot}}(t) \\ \mathbf{Q}_{\text{tot}} & \mathbf{F}_{\text{tot}} \end{bmatrix}$$

are piecewise continuous and locally bounded, and that condition (31) simply becomes

$$\begin{bmatrix} -\mathbf{Q}_{\text{tot}} & -\mathbf{F}_{\text{tot}} \\ -\mathbf{F}_{\text{tot}}^T & \mathbf{C}_{\text{tot}}^{\text{U}} \end{bmatrix} \succeq \begin{bmatrix} -\mathbf{Q}_{\text{tot}} & -\mathbf{F}_{\text{tot}} \\ -\mathbf{F}_{\text{tot}}^T & \mathbf{C}_{\text{tot}}(t) \end{bmatrix} \Longleftrightarrow$$
$$\begin{bmatrix} \mathbf{0} & \mathbf{0} \\ \mathbf{0} & \mathbf{C}_{\text{tot}}^{\text{U}} - \mathbf{C}_{\text{tot}}(t) \end{bmatrix} \succeq \mathbf{0} \iff \mathbf{C}_{\text{tot}}(t) \preceq \mathbf{C}_{\text{tot}}^{\text{U}}, \qquad \text{for } t \in \mathcal{I}$$

where the last equivalence follows from [40, Prop. 8.2.4]. The inequality $\mathbf{C}_{\text{tot}}(t) \preceq \mathbf{C}_{\text{tot}}^{\text{U}}$ for $t \in \mathcal{I}$, implies $\mathbf{P}_{\text{fus}}^{\text{L}}(t) \preceq \mathbf{P}_{\text{fus}}(t)$ for $t \in \mathcal{I} \cap [t_0, +\infty)$. ∎

Proposition 1 states that in order to determine a lower and upper bound for the covariance matrix $\mathbf{P}_{\text{fus}}$, it suffices to determine a lower and upper bound for the matrix $\mathbf{C}_{\text{tot}}(t)$, and to solve two *constant-coefficient* RDEs [(32) and (34)], with the same initial condition $\mathbf{P}_{\text{fus}}(t_0)$.

In order to complete our analysis, let us now derive explicit expressions for the constant matrices $\mathbf{C}_{\text{tot}}^{\text{U}}$ and $\mathbf{C}_{\text{tot}}^{\text{L}}$ appearing in (32) and (34). We have that

$$\mathbf{C}_{\text{tot}}(t) \triangleq \sum_{i=1}^{n} (\mathbf{R}_i^{\text{Car}}(t) + \mathbf{\Delta}_i)^{-1}$$
$$\preceq \frac{1}{4} \sum_{i=1}^{n} \left((\mathbf{R}_i^{\text{Car}}(t))^{-1} + \mathbf{\Delta}_i^{-1} \right)$$
$$\preceq \frac{1}{4} \left(\frac{n}{a_0} \max \left\{ \frac{1}{\alpha_\phi}, \frac{1}{\alpha_\theta}, 1 \right\} \mathbf{I}_{3(m+n)} + \sum_{i=1}^{n} \mathbf{\Delta}_i^{-1} \right)$$
$$\triangleq \mathbf{C}_{\text{tot}}^{\text{U}}$$

where the first inequality follows from [40, Fact 8.10.7], and the second follows from the observation that matrix $\mathbf{T}_i \operatorname{diag}(1/\alpha_\phi, 1/\alpha_\theta, 1) \mathbf{T}_i^T$ is related to $\operatorname{diag}(1/\alpha_\phi, 1/\alpha_\theta, 1)$ by a similarity transformation (notice that $\mathbf{T}_i^T = \mathbf{T}_i^{-1}$, being $\mathbf{T}_i$ a rotation matrix), therefore the two matrices have the same eigenvalues. Analogously, we have that

$$\mathbf{C}_{\text{tot}}(t) \succeq \sum_{i=1}^{n} \frac{1}{\lambda_{\max}(\mathbf{R}_i^{\text{Car}}(t) + \mathbf{\Delta}_i)} \mathbf{I}_{3(m+n)}$$
$$\succeq \sum_{i=1}^{n} \frac{1}{\lambda_{\max}(\mathbf{R}_i^{\text{Car}}(t)) + \lambda_{\max}(\mathbf{\Delta}_i)} \mathbf{I}_{3(m+n)}$$
$$\succeq \sum_{i=1}^{n} \frac{1}{f_r(r_{\text{M}}) \max\{\alpha_\phi, \alpha_\theta, 1\} + \lambda_{\max}(\mathbf{\Delta}_i)} \mathbf{I}_{3(m+n)}$$
$$\triangleq \mathbf{C}_{\text{tot}}^{\text{L}}$$

where the first inequality follows from [40, Corollary 8.4.2], the second from [40, Th. 8.4.11], and r_M indicates the *maximum* vehicle-to-target (or vehicle-to-vehicle) distance that each agent can measure, determined, e.g., by the size of the 3-D navigation environment (cf. [24]).

If we substitute the upper and lower bounds $\mathbf{C}_{tot}^U$, $\mathbf{C}_{tot}^L$ in (32) and (34), and numerically evaluate the solution of the two equations, we obtain a lower and upper bound on $\mathbf{P}_{fus}$ at any instant of time. Since the system under investigation is completely observable, then after undergoing an initial transient phase, $\mathbf{P}_{fus}$ will reach a steady state. It is therefore worth studying the *steady-state behavior* of the uncertainty over the targets' and vehicles' position; this information is conveyed by the *asymptotic solutions* $\mathbf{P}_{fus}^L(\infty)$, $\mathbf{P}_{fus}^U(\infty)$ of (32) and (34). Let the pair $(\mathbf{P}_\star, \mathbf{C}_\star)$ denotes either $(\mathbf{P}_{fus}^L, \mathbf{C}_{tot}^U)$ or $(\mathbf{P}_{fus}^U, \mathbf{C}_{tot}^L)$. From Kalman-filter theory [36, p. 476], we know that if the pair $(\mathbf{F}_{tot}, \mathbf{Q}_{tot}^{1/2})$ is stabilizable, then the solution of

$$\dot{\mathbf{P}}_\star(t) = \mathbf{F}_{tot}\mathbf{P}_\star(t) + \mathbf{P}_\star(t)\mathbf{F}_{tot}^T + \mathbf{Q}_{tot} - \mathbf{P}_\star(t)\mathbf{C}_\star\mathbf{P}_\star(t)$$

converges to a unique positive-definite matrix at steady state from any initial condition $\mathbf{P}_\star(t_0)$, determined by solving the *continuous-time algebraic Riccati equation* (CARE)

$$\mathbf{F}_{tot}\mathbf{P}_\star(\infty) + \mathbf{P}_\star(\infty)\mathbf{F}_{tot}^T + \mathbf{Q}_{tot} - \mathbf{P}_\star(\infty)\mathbf{C}_\star\mathbf{P}_\star(\infty) = \mathbf{0}.$$

Therefore, in summary, the study of the steady-state performance of ACLMT, simply translates into solving two standard CAREs for $\mathbf{P}_{fus}^L(\infty)$ and $\mathbf{P}_{fus}^U(\infty)$, for which efficient numerical routines exist in mathematical software packages.

Note that the bounds described in this section are relative to the uncertainty on the considered target and measurement models, and they are *not* bounds on the (unknown) *globally* optimal trajectory of the vehicles (cf. [16]).

Remark 3 (Bounds on the cost function J): From condition (35) and Weyl's inequality [40, Th. 8.4.9], it follows that for $t \in \mathcal{I} \cap [t_0, +\infty)$:

$$\ln\det(\mathbf{P}_{fus}^L(t)) \leq \ln\det(\mathbf{P}_{fus}(t)) \leq \ln\det(\mathbf{P}_{fus}^U(t)). \quad (36)$$

Therefore, if the pair $(\mathbf{F}_{tot}, \mathbf{Q}_{tot}^{1/2})$ is stabilizable, $\ln\det(\mathbf{P}_{fus}^L(\infty))$ and $\ln\det(\mathbf{P}_{fus}^U(\infty))$ represent steady-state lower and upper bounds on the value of the cost function for the D-optimality criterion. Inequalities analogous to (36) hold with the cost functions (6) and (7) of the A- and E-optimality criteria.

We conclude this section with Proposition 2, which leveraging again the comparison theorem, studies the impact of the process noises $\mathbf{w}_j$ and $\mathbf{n}_i$ on the targets' and vehicles' position uncertainty (cf. [26, Sect. VI]). In order to state the proposition, let us partition the matrix $\mathbf{P}_{fus}$ as

$$\mathbf{P}_{fus} = \begin{bmatrix} \mathbf{P}_{TT} & \mathbf{P}_{TV} \\ \mathbf{P}_{VT} & \mathbf{P}_{VV} \end{bmatrix}$$

where $\mathbf{P}_{TT} \in \mathbb{R}^{3m \times 3m}$ is the covariance matrix corresponding to the *targets'* position estimate, $\mathbf{P}_{VV} \in \mathbb{R}^{3n \times 3n}$ is the covariance matrix relative to the *vehicles'* position estimate, and $\mathbf{P}_{TV} \in \mathbb{R}^{3m \times 3n}$ is the cross-correlation matrix between the targets and vehicles (obviously, $(\mathbf{P}_{TV})^T = \mathbf{P}_{VT}$).

Proposition 2 (Bounds on $\mathbf{P}_{TT}$ and $\mathbf{P}_{VV}$): Let $\mathcal{I} \subset \mathbb{R}_{\geq 0}$ be some interval, and $t_0 \in \mathcal{I}$. Let $\mathbf{P}_{fus}'$ and $\mathbf{P}_{fus}$ be the solutions of the following RDEs on $\mathcal{I}$:

$$\dot{\mathbf{P}}_{fus}' = \mathbf{F}_{tot}\mathbf{P}_{fus}' + \mathbf{P}_{fus}'\mathbf{F}_{tot}^T - \mathbf{P}_{fus}'\mathbf{C}_{tot}(t)\mathbf{P}_{fus}'$$
$$+\text{blkdiag}(\mathbf{Q}_1, \ldots, \mathbf{Q}_m, \mathbf{N}_1, \ldots, \mathbf{N}_i', \ldots, \mathbf{N}_n)$$
$$\dot{\mathbf{P}}_{fus} = \mathbf{F}_{tot}\mathbf{P}_{fus} + \mathbf{P}_{fus}\mathbf{F}_{tot}^T - \mathbf{P}_{fus}\mathbf{C}_{tot}(t)\mathbf{P}_{fus}$$
$$+\text{blkdiag}(\mathbf{Q}_1, \ldots, \mathbf{Q}_m, \mathbf{N}_1, \ldots, \mathbf{N}_i, \ldots, \mathbf{N}_n) \quad (37)$$

with $\mathbf{P}_{fus}'(t_0) = \mathbf{P}_{fus}(t_0)$, and $\mathbf{P}_{fus}(t_0)$ symmetric. Then, if $\mathbf{N}_i' \succeq \mathbf{N}_i$ for a certain $i \in \{1, \ldots, n\}$, we have that $\mathbf{P}_{TT}'(t) \succeq \mathbf{P}_{TT}(t)$ for $t \in \mathcal{I} \cap [t_0, +\infty)$.

Analogously, let $\mathbf{P}_{fus}'$ and $\mathbf{P}_{fus}$ be the solutions of the following RDEs on $\mathcal{I}$:

$$\dot{\mathbf{P}}_{fus}' = \mathbf{F}_{tot}\mathbf{P}_{fus}' + \mathbf{P}_{fus}'\mathbf{F}_{tot}^T - \mathbf{P}_{fus}'\mathbf{C}_{tot}(t)\mathbf{P}_{fus}'$$
$$+\text{blkdiag}(\mathbf{Q}_1, \ldots, \mathbf{Q}_j', \ldots, \mathbf{Q}_m, \mathbf{N}_1, \ldots, \mathbf{N}_n)$$
$$\dot{\mathbf{P}}_{fus} = \mathbf{F}_{tot}\mathbf{P}_{fus} + \mathbf{P}_{fus}\mathbf{F}_{tot}^T - \mathbf{P}_{fus}\mathbf{C}_{tot}(t)\mathbf{P}_{fus}$$
$$+\text{blkdiag}(\mathbf{Q}_1, \ldots, \mathbf{Q}_j, \ldots, \mathbf{Q}_m, \mathbf{N}_1, \ldots, \mathbf{N}_n)$$

with $\mathbf{P}_{fus}'(t_0) = \mathbf{P}_{fus}(t_0)$ and $\mathbf{P}_{fus}(t_0)$ symmetric. Then, if $\mathbf{Q}_j' \succeq \mathbf{Q}_j$ for a certain $j \in \{1, \ldots, m\}$, we have that $\mathbf{P}_{VV}'(t) \succeq \mathbf{P}_{VV}(t)$ for $t \in \mathcal{I} \cap [t_0, +\infty)$.

Proof: If $\mathbf{N}_i' \succeq \mathbf{N}_i$ for a certain $i \in \{1, \ldots, n\}$, the application of Theorem 1 to the RDEs in (37) leads to the condition

$$\mathbf{Y}(t) \triangleq \begin{bmatrix} \mathbf{P}_{TT}'(t) - \mathbf{P}_{TT}(t) & \mathbf{P}_{TV}'(t) - \mathbf{P}_{TV}(t) \\ \mathbf{P}_{VT}'(t) - \mathbf{P}_{VT}(t) & \mathbf{P}_{VV}'(t) - \mathbf{P}_{VV}(t) \end{bmatrix} \succeq \mathbf{0} \quad (38)$$

for $t \in \mathcal{I} \cap [t_0, +\infty)$. From the property of the Schur complement of $\mathbf{P}_{TT}' - \mathbf{P}_{TT}$ with respect to $\mathbf{Y}$ [40, Prop. 8.2.4, ii)], (38) implies $\mathbf{P}_{TT}' - \mathbf{P}_{TT} \succeq \mathbf{0}$, i.e., $\mathbf{P}_{TT}' \succeq \mathbf{P}_{TT}$. The second part of the statement can be proved in an analogous way, by considering the Schur complement of $\mathbf{P}_{VV}' - \mathbf{P}_{VV}$ with respect to $\mathbf{Y}$. ∎

Proposition 2 states that an increase in the velocity uncertainty for one of the vehicles ($\mathbf{N}_i' \succeq \mathbf{N}_i$), leads to an uncertainty growth in the targets' position ($\mathbf{P}_{TT}' \succeq \mathbf{P}_{TT}$). Vice versa, an increase in the velocity uncertainty for one of the targets ($\mathbf{Q}_j' \succeq \mathbf{Q}_j$), directly translates into an uncertainty growth in the vehicles' position ($\mathbf{P}_{VV}' \succeq \mathbf{P}_{VV}$).

V. SIMULATION EXPERIMENTS

Extensive simulation experiments have been performed to illustrate the theory presented in the previous sections. In all our tests we used the cost function for the D-optimality criterion to design the gradient controller, because of its invariance under any nonsingular reparametrization [19, Sec. 6.1]. In the simulations, the initial velocity $\mathbf{q}_i(t_0) = \mathbf{q}_i(0)$ of the aerial vehicles is set to zero.

Fig. 4(a) shows the trajectory of four aerial vehicles *cooperatively tracking* tracking a target whose motion is governed by (1), with $\mathbf{F} = -5\,\text{diag}(10^{-3}, 10^{-4}, 10^{-2})$, $\mathbf{G} = \mathbf{I}_3$, $\mathbf{u}_T(t) = [0, -10^{-2}, 0]^T$ and $\mathbf{Q} = 0.07\,\mathbf{I}_3$. The initial positions of the agents and target are, $\mathbf{p}_1(0) = [-3, 15, 0]^T$, $\mathbf{p}_2(0) = [3, 15, 0]^T$, $\mathbf{p}_3(0) = [0, 15, 5]^T$, $\mathbf{p}_4(0) = [0, 15, -5]^T$, $\mathbf{x}(0) = [0, 12, 0]^T$ and are respectively marked with circles
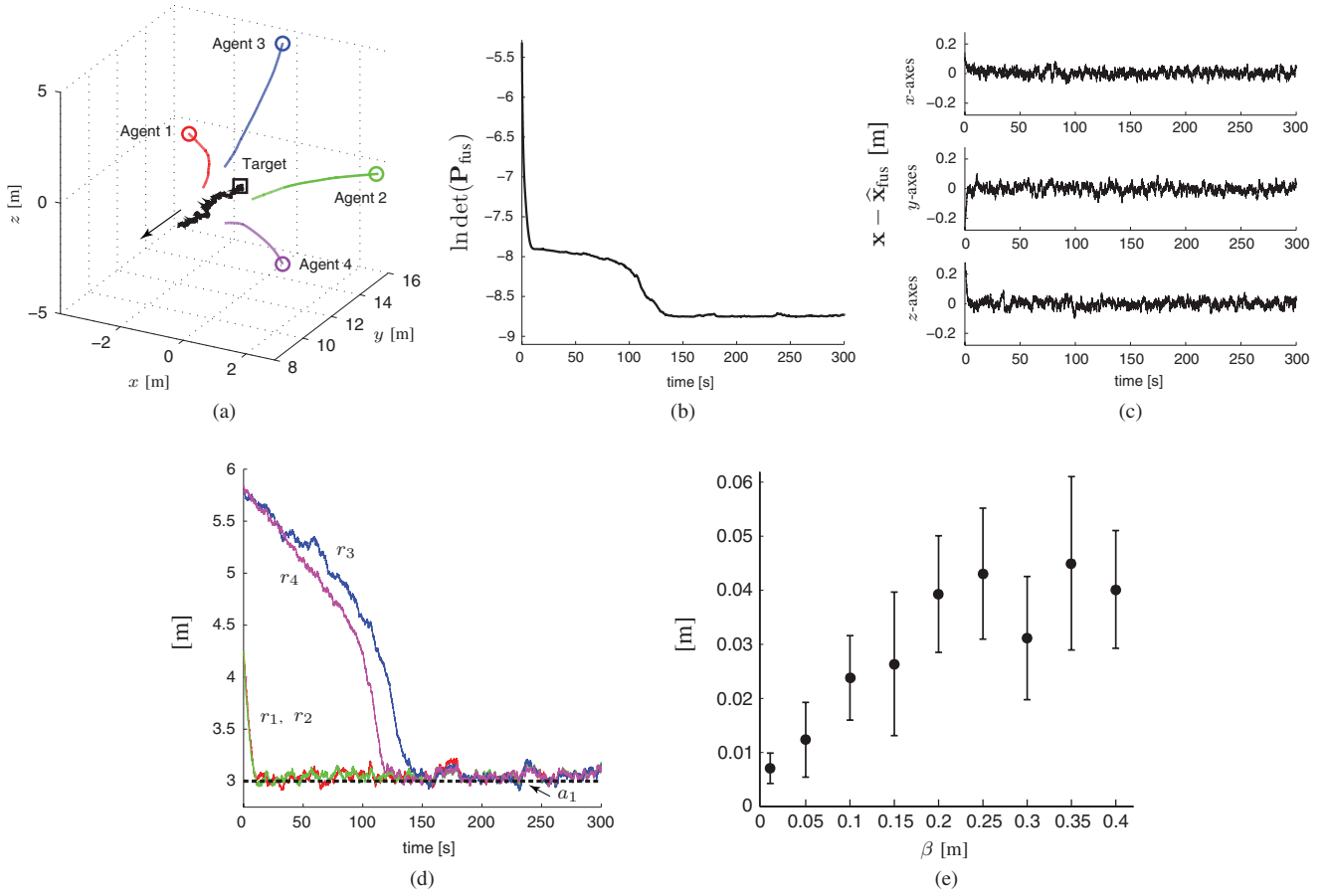
Fig. 4. *Cooperative active target tracking*. (a) Trajectory of the four agents (colored lines) and of the target (black line). The initial positions are marked with circles and a square, respectively, and the direction of motion of the target is indicated with an arrow. (b) Time history of the cost function $J = \ln\det(\mathbf{P}_{\mathrm{fus}})$. (c) Time evolution of the estimation error $\mathbf{x} - \widehat{\mathbf{x}}_{\mathrm{fus}}$. (d) Time history of r_i, $i \in \{1, \ldots, 4\}$ (colored line) and $a_1 = 3$ m (black dashed line). (e) Mean and standard deviation of $\|\mathbf{x}(T_{\mathrm{fin}}) - \widehat{\mathbf{x}}_{\mathrm{fus}}(T_{\mathrm{fin}})\|_2$, $T_{\mathrm{fin}} = 300$ s, over ten trials for $\mathbf{Q} = \beta^2\,\mathbf{I}_3$, $\beta \in \{0.01, 0.05, 0.1, 0.15, 0.2, \ldots, 0.4\}$.
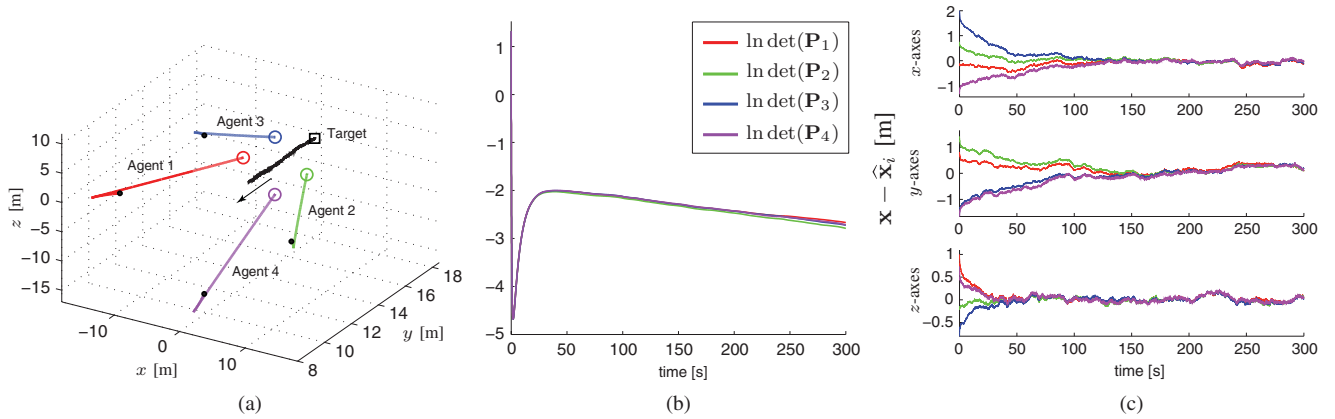

Fig. 5. *Noncooperative active target tracking*. (a) Trajectory of the four agents (colored line) and of the target (black line). The initial initial and final positions of the agents are marked with circles and black dots, respectively, while the initial position of the target is marked with a square. (b) Time history of the cost functions $J_i = \ln\det(\mathbf{P}_i)$, $i \in \{1, \ldots, 4\}$. (c) Time evolution of the estimation errors $\mathbf{x} - \widehat{\mathbf{x}}_i$, $i \in \{1, \ldots, 4\}$: *red* agent 1, *green* agent 2, *blue* agent 3, *magenta* agent 4.

and a square in Fig. 4(a). The parameters of the measurement model are $a_0 = a_2 = 0.2$, $a_1 = 3$, $\alpha_\theta = \alpha_\phi = 0.8$, and the gain and damping matrices are $\mathbf{\Gamma} = 0.5\,\mathbf{I}_3$ and $\mathbf{B} = 2\,\mathbf{I}_3$, respectively. Fig. 4(b) reports the time history of $J = \ln\det(\mathbf{P}_{\mathrm{fus}})$ and Fig. 4(c) reports the target's estimation error $\mathbf{x} - \widehat{\mathbf{x}}_{\mathrm{fus}}$. Fig. 4(d) displays the time evolution of r_i, $i \in \{1, \ldots, 4\}$ (colored lines).

Note that after about 150 s all the vehicles reach their sweet spot located at a distance $a_1 = 3$ m from the target (black dashed line). It is also worth mentioning that although the "small-angle condition" is violated here (recall Remark 1), in this as well as in many other simulation experiments, we never experienced a significant performance degradation of our

algorithm. Finally, Fig. 4(e) shows the influence of the process noise $\mathbf{w}(t)$ on the steady-state target's estimation error. In particular, in the figure, we have reported the mean and standard deviation of $\|\mathbf{x}(T_{\text{fin}}) - \widehat{\mathbf{x}}_{\text{fus}}(T_{\text{fin}})\|_2$, ($T_{\text{fin}} = 300$ s is the final simulation time), over ten trials for increasing process-noise power: $\mathbf{Q} = \beta^2 \mathbf{I}_3$, $\beta \in \{0.01, 0.05, 0.1, 0.15, 0.2, \ldots, 0.4\}$. For consistency, in all the trials, we used the same initialization for the Kalman filter: $\widehat{\mathbf{x}}_{\text{fus}}(0) = \mathbf{x}^T(0) + [1, -3, -2]^T$, $\mathbf{P}_{\text{fus}}(0) = \mathbf{I}_3$.

Fig. 5(a) shows the trajectory of four aerial vehicles tracking a target and adopting the *noncooperative estimation-and-control strategy* described in Section II-D (for improving readability, the initial and final position of the agents is marked here with circles and black dots, respectively). The same parameters as those in Fig. 4(a)–(d) have been used in Fig. 5, the only difference being represented by the initial position of the vehicles and target, and by the gain and damping matrices, that are, respectively, $\mathbf{p}_1(0) = [-5, 15, 0]^T$, $\mathbf{p}_2(0) = [5, 15, 0]^T$, $\mathbf{p}_3(0) = [0, 15, 5]^T$, $\mathbf{p}_4(0) = [0, 15, -5]^T$, $\mathbf{x}(0) = [0, 18, 0]^T$ and $\mathbf{\Gamma} = 23\,\mathbf{I}_3$, $\mathbf{B} = 15\,\mathbf{I}_3$. Fig. 5(b) reports the time history of the cost functions $J_i = \ln \det(\mathbf{P}_i)$, $i \in \{1, \ldots, 4\}$, and Fig. 5(c) the time evolution of the estimation errors $\mathbf{x} - \widehat{\mathbf{x}}_i$, $i \in \{1, \ldots, 4\}$, (*red* agent 1, *green* agent 2, *blue* agent 3, and *magenta* agent 4). In Fig. 5(b), we observe an agreement on the value of the cost functions J_i, $i \in \{1, \ldots, 4\}$ (corresponding to the existence of a feedback Nash equilibrium solution, cf. Section II-D), and from a comparison of Figs. 5(b) and 4(b), we notice, as expected, that the individual estimates of the target's position are poorer than the estimate obtained by fusing the measurements of the four agents.

Fig. 6(a) shows the trajectory of two targets and three vehicles performing ACLMT. In (25) and (26), we chose $\mathbf{F}_1 = \mathbf{F}_2 = -\text{diag}(10^{-3}, 10^{-3}, 10^{-4})$, $\mathbf{G}_1 = \mathbf{G}_2 = \mathbf{I}_3$, $\mathbf{u}_{\text{T1}} = [-0.7, -0.01, -0.01]^T$, $\mathbf{u}_{\text{T2}} = [-0.7, 0.03, -0.01]^T$, $\mathbf{Q}_1 = \mathbf{Q}_2 = 0.05\,\mathbf{I}_3$, $\mathbf{N}_1 = \mathbf{N}_2 = \mathbf{N}_3 = 0.03\,\mathbf{I}_3$ and $\mathbf{D}_1 = \mathbf{D}_2 = \mathbf{D}_3 = 0.05\,\mathbf{I}_3$. The initial positions of the agents and targets are $\mathbf{p}_1(0) = [-3, 18, 0]^T$, $\mathbf{p}_2(0) = [-3, 10, -2]^T$, $\mathbf{p}_3(0) = [6, 5, 1]^T$ and $\mathbf{x}_1(0) = [-5, 12, 1]^T$, $\mathbf{x}_2(0) = [-5, 2, 4]^T$. The parameters of the measurement model are $a_0 = a_2 = 0.2$, $a_1 = 5$, $\alpha_\theta = \alpha_\phi = 1$ and the gain matrix $\mathbf{\Gamma} = 0.09\,\mathbf{I}_3$. For the sake of illustration, we chose the following simple association matrix:

$$\mathbf{\Lambda}(\mathbf{x}_{\text{tot}}(t)) = \begin{bmatrix} 1 & 0 & 0 & 0 & 0 \\ 1/2 & 1/2 & 0 & 0 & 0 \\ 0 & 1 & 0 & 0 & 0 \end{bmatrix}, \quad \forall t \geq 0.$$

In this way, the first agent is assigned to the first target, the third agent to the second target, and the second agent to both targets. Fig. 6(b) shows the time history of $\ln \det(\mathbf{P}_{\text{fus}})$ (solid line), $\ln \det(\mathbf{P}_{\text{fus}}^{\text{L}})$ (dotted line) and $\ln \det(\mathbf{P}_{\text{fus}}^{\text{U}})$ (dashed line); to generate this plot, we chose $r_{\text{M}} = 12$ m. In Fig. 6(c) and (d), the estimation errors $\mathbf{x}_{\text{tot}}(1{:}3) - \widehat{\mathbf{x}}_{\text{fus}}(1{:}3)$ and $\mathbf{x}_{\text{tot}}(4{:}6) - \widehat{\mathbf{x}}_{\text{fus}}(4{:}6)$ (red solid line) of the first and second target, respectively, are compared against the $\pm 3\sigma$ enveloping lines associated with the actual position estimate's covariance matrix (black solid line), and with the theoretical lower and upper bounds for $\mathbf{P}_{\text{fus}}$ (black dotted and dashed lines,

respectively); similar position estimation errors were obtained for the three vehicles (not shown in Fig. 6).

Fig. 6(e) and (f) have been generated using the same parameters and initial conditions as those in Fig. 6(a)–(d), and they illustrate Proposition 2. Actually, Fig. 6(e) shows the time history of the eigenvalues of the matrix $\mathbf{P}'_{\text{TT}} - \mathbf{P}_{\text{TT}} \in \mathbf{R}^{6 \times 6}$ where $\mathbf{P}'_{\text{TT}}$ corresponds to $\mathbf{N}'_2 = 1.05\,\mathbf{I}_3$ and $\mathbf{P}_{\text{TT}}$ to $\mathbf{N}_2 = 0.03\,\mathbf{I}_3$ [note that there are only two distinct curves in Fig. 6(e), since some of the eigenvalues coalesce]. Analogously, Fig. 6(f) reports the time history of the eigenvalues of the matrix $\mathbf{P}'_{\text{VV}} - \mathbf{P}_{\text{VV}} \in \mathbf{R}^{9 \times 9}$, where $\mathbf{P}'_{\text{VV}}$ corresponds to $\mathbf{Q}'_1 = 1.05\,\mathbf{I}_3$ and $\mathbf{P}_{\text{VV}}$ to $\mathbf{Q}_1 = 0.05\,\mathbf{I}_3$. As it is evident from the two figures, the eigenvalues of $\mathbf{P}'_{\text{TT}} - \mathbf{P}_{\text{TT}}$ and $\mathbf{P}'_{\text{VV}} - \mathbf{P}_{\text{VV}}$ are nonnegative at all times, and hence $\mathbf{P}'_{\text{TT}}(t) \succeq \mathbf{P}_{\text{TT}}(t)$ and $\mathbf{P}'_{\text{VV}}(t) \succeq \mathbf{P}_{\text{VV}}(t)$ for all $t \geq 0$, as predicted by Proposition 2.

In Fig. 6(g), we compared the performance of our basic cooperative active target-tracking algorithm (the positions of the vehicles are perfectly known here), with ACLMT, under equivalent conditions. The figure, in particular, shows the time history of the estimation error of a single target, obtained by four vehicles using the two approaches (black and red lines, respectively), with $\mathbf{\Gamma} = 0.05\,\mathbf{I}_3$, $\mathbf{B} = 50\,\mathbf{I}_3$ (for the former method), $a_0 = a_2 = 0.2$, $a_1 = 5$, $\alpha_\theta = \alpha_\phi = 1$ and initial conditions, $\mathbf{p}_1(0) = [0, 14, -3]^T$, $\mathbf{p}_2(0) = [3, 13, 0]^T$, $\mathbf{p}_3(0) = [-1, 11, 5]^T$, $\mathbf{p}_4(0) = [1, 9, -2]^T$, $\mathbf{x}_1(0) = [0, 12, 0]^T$. For ACLMT we chose $\mathbf{F}_1 = -0.5\,\text{diag}(10^{-2}, 10^{-3}, 10^{-2})$, $\mathbf{G}_1 = \mathbf{I}_3$, $\mathbf{u}_{\text{T1}} = [0, -0.01, 0]^T$, $\mathbf{Q}_1 = 0.07\,\mathbf{I}_3$, $\mathbf{N}_1 = \cdots = \mathbf{N}_4 = 0.15\,\mathbf{I}_3$, $\mathbf{D}_1 = \cdots = \mathbf{D}_4 = 0.5\,\mathbf{I}_3$, and

$$\mathbf{\Lambda}(\mathbf{x}_{\text{tot}}(t)) = \begin{bmatrix} 1 & 0 & 0 & 0 & 0 \\ 1 & 0 & 0 & 0 & 0 \\ 1 & 0 & 0 & 0 & 0 \\ 1 & 0 & 0 & 0 & 0 \end{bmatrix}, \quad \forall t \geq 0.$$

Finally, the Kalman filter was initialized with $\widehat{\mathbf{x}}_{\text{fus}}(0) = \mathbf{x}_1^T(0) + [1, -3, -2]^T$, $\mathbf{P}_{\text{fus}}(0) = \mathbf{I}_3$, and $\widehat{\mathbf{x}}_{\text{fus}}(0) = [\mathbf{x}_1^T(0) + [1, -3, -2]^T, \mathbf{p}_1^T(0), \mathbf{p}_2^T(0), \mathbf{p}_3^T(0), \mathbf{p}_4^T(0)]^T$, $\mathbf{P}_{\text{fus}}(0) = \mathbf{I}_{15}$, respectively. From Fig. 6(g), we observe that although the transient performance of ACLMT is worse than that of the basic cooperative active target-tracking algorithm, the steady-state target's estimation errors of the two approaches are comparable.

Finally, Fig. 7(a)–(c) illustrate the influence of the parameters $\alpha_\theta = \alpha_\phi \in \{0.05, 0.1, 0.25, 0.5, \ldots, 2\}$, $a_0 \in \{0.01, 0.05, 0.25, 0.5, \ldots, 1\}$ and $\mathbf{\Delta}_1 = \mathbf{\Delta}_2 = \mathbf{\Delta}_3 = \gamma\,\mathbf{I}_{15}$, $\gamma \in \{0.05, 0.075, 0.1, 0.25, 0.5, \ldots, 1\}$, on the bounds $\ln \det(\mathbf{P}_{\text{fus}}^{\text{L}})$ and $\ln \det(\mathbf{P}_{\text{fus}}^{\text{U}})$ (dotted and dashed lines, respectively) in ACLMT. Fig. 7(a)–(c) were obtained using the same simulation parameters as those in Fig. 6(a)–(f), and initializing the Kalman filter with $\widehat{\mathbf{x}}_{\text{fus}}(0) = [\mathbf{x}_1^T(0), \mathbf{x}_2^T(0), \mathbf{p}_1^T(0), \mathbf{p}_2^T(0), \mathbf{p}_3^T(0)]^T$, $\mathbf{P}_{\text{fus}}(0) = \mathbf{I}_{15}$. From the figures, it comes as no surprise that the smaller α_θ, α_ϕ, a_0, and the "smaller" $\mathbf{\Delta}_1$, $\mathbf{\Delta}_2$, $\mathbf{\Delta}_3$, the higher is the steady-state estimation accuracy of the target's position.

VI. Conclusion and Future Work

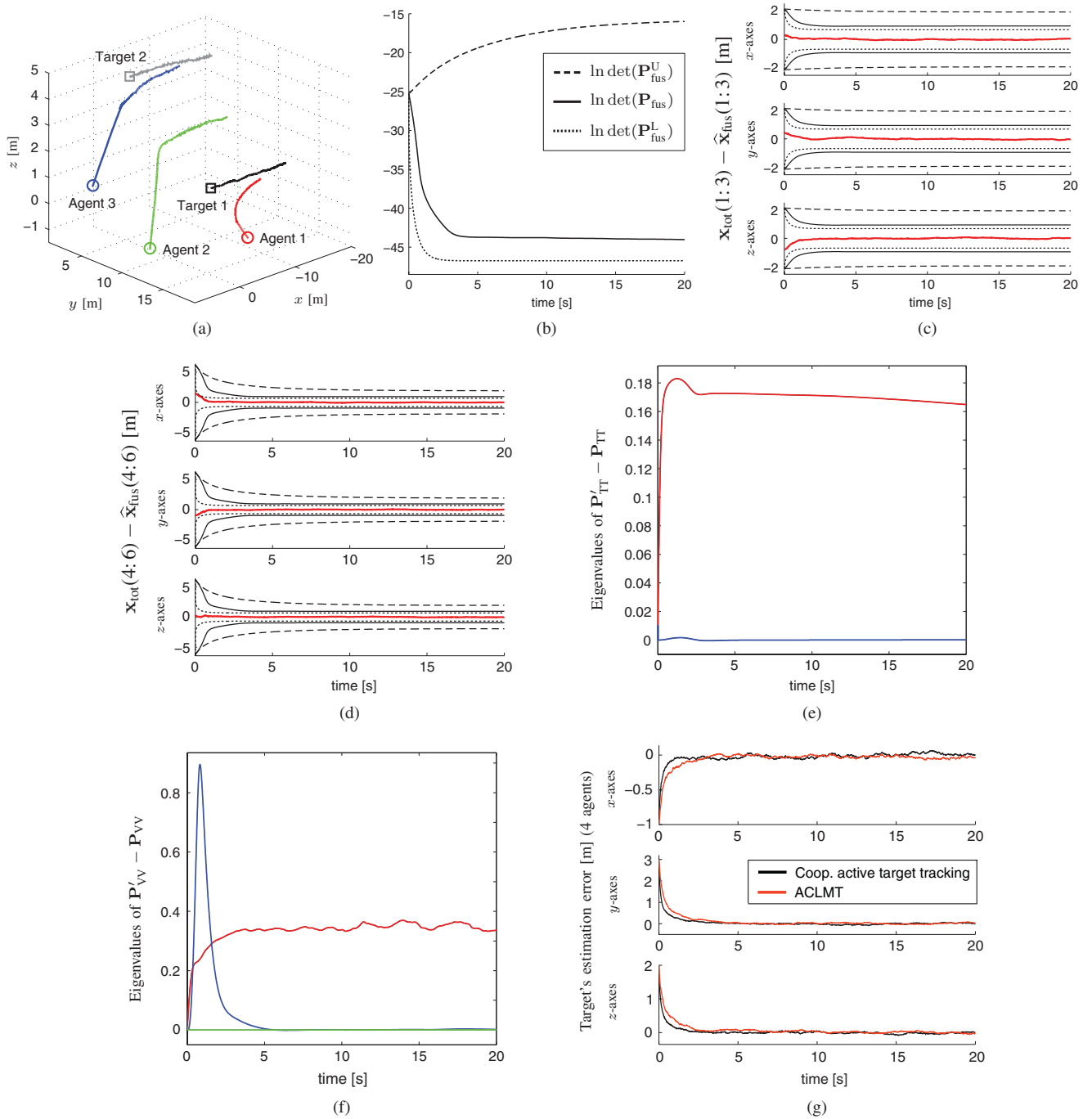In this paper, we have proposed an active target-tracking strategy to deploy a team of unmanned aerial vehicles along

Fig. 6. *ACLMT*. (a) Trajectory of the three agents (colored lines) and of the two targets (black and gray lines); the initial positions are marked with circles and squares, respectively. (b) Time history of the cost function $J = \ln \det(\mathbf{P}_{\text{fus}})$ (solid line), $\ln \det(\mathbf{P}_{\text{fus}}^{\text{L}})$ (dotted line), and $\ln \det(\mathbf{P}_{\text{fus}}^{\text{L}})$ (dashed line). (c) and (d) Time evolution of the estimation errors $\mathbf{x}_{\text{tot}}(1{:}3) - \widehat{\mathbf{x}}_{\text{fus}}(1{:}3)$ and $\mathbf{x}_{\text{tot}}(4{:}6) - \widehat{\mathbf{x}}_{\text{fus}}(4{:}6)$ of the first and second target, respectively (red solid lines), and $\pm 3\sigma$ enveloping lines associated with the actual estimate's error covariance matrix (black solid lines) and with the theoretical lower and upper bounds ((black dotted and dashed lines, respectively). (e) Time history of the eigenvalues of $\mathbf{P}_{\text{TT}}' - \mathbf{P}_{\text{TT}} \in \mathbb{R}^{6\times 6}$. (f) Time history of the eigenvalues of $\mathbf{P}_{\text{VV}}' - \mathbf{P}_{\text{VV}} \in \mathbb{R}^{9\times 9}$. (g) Time evolution of the position estimation error of a single target obtained by four agents using our basic cooperative active target-tracking algorithm (black lines; the position of the agents is perfectly known) and ACLMT (red lines).

paths that minimize the uncertainty about the position of a moving target. Both *cooperative* and *noncooperative* scenarios have been explored, and a new problem, called ACLMT has been introduced. In this problem, the aerial vehicles relocate themselves in the 3-D space in order to maximize both the accuracy of their *own position estimate* and that of *multiple moving targets*. For ACLMT, the monotonicity property of the Riccati differential equation arising from the Kalman–Bucy

filter, which describes the propagation of the targets'/vehicles' position uncertainty through time, allowed us to determine guaranteed performance bounds for our algorithm. The proposed theoretical results have been illustrated via extensive numerical simulations.

There is a series of interesting open issues that this paper has not tackled. First, in future research, we are going to extend the proposed results to heterogeneous teams of ground and
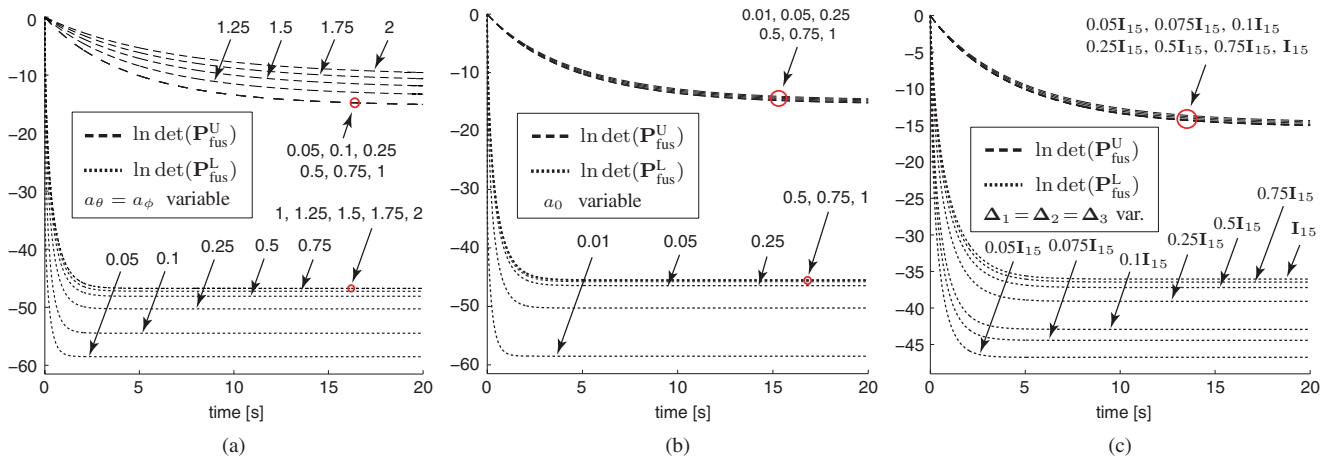
Fig. 7. *ACLMT.* Influence of the parameters (a) $a_\theta = a_\phi$, (b) a_0, and (c) $\boldsymbol{\Delta}_1 = \boldsymbol{\Delta}_2 = \boldsymbol{\Delta}_3$, on the bounds $\ln \det(\mathbf{P}_{\text{fus}}^{\text{L}})$ and $\ln \det(\mathbf{P}_{\text{fus}}^{\text{U}})$ (dotted and dashed lines, respectively).

aerial robots (e.g., more realistically modeled as nonholonomic vehicles, cf. [41]), and to take advantage of the performance analysis of Section IV to synthesize more efficient controllers for ACLMT. We also aim to study the impact of team topology on the target's estimation accuracy in the case of limited inter-vehicle communication [25], and to test the proposed approach on real flying platforms (e.g., on commercial quadrotors [42]). Finally, in future works, we will consider more sophisticated assignment algorithms for ACLMT in the case of exteroceptive sensors with limited range and/or aperture and cluttered environments [43]–[46], we will analyze the stability of the full closed-loop system in terms of the controller's parameters (cf. [10]), and we will investigate convex approximations to the cost functions (5)–(7), by exploiting the concavity property of the Riccati differential equation of the Kalman–Bucy filter.

REFERENCES

[1] V. Kumar, D. Rus, and G. S. Sukhatme, "Networked robots," in *Handbook of Robotics*, B. Siciliano and O. Khatib, Eds. New York: Springer-Verlag, 2008, ch. 41, pp. 943–958.

[2] F. Bullo, J. Cortés, and S. Martínez, *Distributed Control of Robotic Networks*. Princeton, NJ: Princeton Univ. Press, 2009.

[3] M. Mesbahi and M. Egerstedt, *Graph Theoretic Methods in Multiagent Networks*. Princeton, NJ: Princeton Univ. Press, 2010.

[4] Y. Bar-Shalom, X. R. Li, and T. Kirubarajan, *Estimation with Applications to Tracking and Navigation*. New York: Wiley, 2001.

[5] C. Taylor, A. Rahimi, J. Bachrach, H. Shrobe, and A. Grue, "Simultaneous localization, calibration, and tracking in an ad hoc sensor network," in *Proc. 5th ACM Int. Conf. Inf. Process. Sensors Netw.*, 2006, pp. 27–33.

[6] D. Uciński, *Optimal Measurement Methods for Distributed Parameter System Identification*. Boca Raton, FL: CRC, 2005.

[7] T. H. Chung, J. W. Burdick, and R. M. Murray, "A decentralized motion coordination strategy for dynamic target tracking," in *Proc. IEEE Int. Conf. Robot. Autom.*, Mar. 2006, pp. 2416–2422.

[8] P. Yang, R. A. Freeman, and K. M. Lynch, "Distributed cooperative active sensing using consensus filters," in *Proc. IEEE Int. Conf. Robot. Autom.*, Jun. 2007, pp. 405–410.

[9] R. Olfati-Saber, "Distributed tracking for mobile sensor networks with information-driven mobility," in *Proc. Amer. Control Conf.*, 2007, pp. 4606–4612.

[10] R. Olfati-Saber and P. Jalalkamali, "Coupled distributed estimation and control for mobile sensor networks," *IEEE Trans. Autom. Control*, vol. 57, no. 10, pp. 2609–2614, Oct. 2012.

[11] K. Zhou and S. I. Roumeliotis, "Optimal motion strategies for range-only constrained multisensor target tracking," *IEEE Trans. Robot.*, vol. 24, no. 5, pp. 1168–1185, Oct. 2008.

[12] K. Zhou and S. I. Roumeliotis, "Multirobot active target tracking with combinations of relative observations," *IEEE Trans. Robot.*, vol. 27, no. 4, pp. 678–695, Aug. 2011.

[13] A. W. Stroupe and T. Balch, "Value-based action selection for observation with robot teams using probabilistic techniques," *Robot. Auton. Syst.*, vol. 50, nos. 2–3, pp. 85–97, 2005.

[14] S. Martínez and F. Bullo, "Optimal sensor placement and motion coordination for target tracking," *Automatica*, vol. 42, no. 4, pp. 661–668, 2006.

[15] F. Zhao, J. Shin, and J. Reich, "Information-driven dynamic sensor collaboration for tracking applications," *IEEE Signal Process. Mag.*, vol. 19, no. 2, pp. 61–72, Feb. 2002.

[16] A. Singh, A. Krause, C. Guestrin, and W. Kaiser, "Efficient informative sensing using multiple robots," *J. Artif. Intell. Res.*, vol. 34, no. 1, pp. 707–755, 2009.

[17] B. Grocholsky, J. Keller, V. Kumar, and G. Pappas, "Cooperative air and ground surveillance," *IEEE Robot. Autom. Mag.*, vol. 13, no. 3, pp. 16–25, Mar. 2006.

[18] E. Stump, V. Kumar, B. Grocholsky, and P. M. Shiroma, "Control for localization of targets using range-only sensors," *Int. J. Robot. Res.*, vol. 28, no. 6, pp. 743–757, 2009.

[19] E. Walter and L. Pronzato, *Identification of Parametric Models*. New York: Springer-Verlag, 1994.

[20] J. M. Passerieux and D. Van Cappel, "Optimal observer maneuver for bearings-only tracking," *IEEE Trans. Aerosp. Electron. Syst.*, vol. 34, no. 3, pp. 777–788, Jul. 1998.

[21] R. Olfati-Saber, "Distributed Kalman filter with embedded consensus filters," in *Proc. 44th IEEE Conf. Decision Control*, Jul. 2005, pp. 8179–8184.

[22] B. I. Triplett, D. J. Klein, and K. A. Morgansen, "Cooperative estimation for coordinated target tracking in a cluttered environment," *Mobile Netw. Appl.*, vol. 14, no. 3, pp. 336–349, 2009.

[23] S. A. P. Quintero, F. Papi, D. J. Klein, L. Chisci, and J. P. Hespanha, "Optimal UAV coordination for target tracking using dynamic programming," in *Proc. 49th IEEE Conf. Decision Control*, Nov. 2010, pp. 4541–4546.

[24] A. I. Mourikis and S. I. Roumeliotis, "Predicting the performance of cooperative simultaneous localization and mapping (C-SLAM)," *Int. J. Robot. Res.*, vol. 25, no. 12, pp. 1273–1286, 2006.

[25] A. I. Mourikis and S. I. Roumeliotis, "Performance analysis of multirobot cooperative localization," *IEEE Trans. Robot.*, vol. 22, no. 4, pp. 666–681, Aug. 2006.

[26] F. M. Mirzaei, A. I. Mourikis, and S. I. Roumeliotis, "On the performance of multirobot target tracking," in *Proc. IEEE Int. Conf. Robot. Autom.*, Dec. 2007, pp. 3482–3489.

[27] R. Sim and N. Roy, "Global A-optimal robot exploration in SLAM," in *Proc. IEEE Int. Conf. Robot. Autom.*, 2005, pp. 661–666.

[28] J. Djugash and S. Singh, "Motion-aided network SLAM with range," *Int. J. Robot. Res.*, vol. 31, no. 5, pp. 604–625, 2012.

[29] A. Cristofaro, A. Renzaglia, and A. Martinelli, "Distributed information filters for MAV cooperative localization," in *Distributed Autonomous Robotic Systems*, vol. 83, A. Martinoli, F. Mondada, N. Correll, G. Mermoud, M. Egerstedt, M. A. Hsieh, L. E. Parker, and K. Støy, Eds. New York: Springer-Verlag, 2010, pp. 133–146.

[30] F. Morbidi and G. L. Mariottini, "On active target tracking and cooperative localization for multiple aerial vehicles," in *Proc. IEEE/RSJ Int. Conf. Intell. Robots Syst.*, Dec. 2011, pp. 2229–2234.

[31] K. V. Ramachandra, *Kalman Filtering Techniques for Radar Tracking*. Boca Raton, FL: CRC, 2000.

[32] S. Gowal, A. Prorok, and A. Martinoli, "Two-phase online calibration for infrared-based inter-robot positioning modules," in *Proc. IEEE/RSJ Int. Conf. Intell. Robots Syst.*, Nov. 2011, pp. 3313–3319.

[33] T. H. Chung, V. Gupta, J. W. Burdick, and R. M. Murray, "On a decentralized active sensing strategy using mobile sensor platforms in a network," in *Proc. 43rd IEEE Conf. Decision Control*, Jun. 2004, pp. 1914–1919.

[34] X. Chen, H. Qi, L. Qi, and K. L. Teo, "Smooth convex approximation to the maximum eigenvalue function," *J. Global Optim.*, vol. 30, no. 2, pp. 253–270, 2004.

[35] E. Polak, *Optimization: Algorithms and Consistent Approximations*. New York: Springer-Verlag, 1997.

[36] R. F. Stengel, *Optimal Control and Estimation*. New York: Dover, 1994.

[37] H. Abou-Kandil, G. Freiling, V. Ionescu, and G. Jank, *Matrix Riccati Equations: In Control and Systems Theory*. Boston, MA: Birkhäuser, 2003.

[38] A. W. Starr and Y. C. Ho, "Nonzero-sum differential games," *J. Optim. Theory Appl.*, vol. 3, no. 3, pp. 184–206, 1969.

[39] T. Başar and G. J. Olsder, *Dynamic Noncooperative Game Theory*, 1st ed. New York: Academic, 1982.

[40] D. S. Bernstein, *Matrix Mathematics: Theory, Facts, and Formulas*. Princeton, NJ: Princeton Univ. Press, 2009.

[41] F. Morbidi, C. Ray, and G. L. Mariottini, "Cooperative active target tracking for heterogeneous robots with application to gait monitoring," in *Proc. IEEE/RSJ Int. Conf. Intell. Robots Syst.*, Jul. 2011, pp. 3608–3613.

[42] V. Kumar and N. Michael, "Opportunities and challenges with autonomous micro aerial vehicles," *Int. J. Robot. Res.*, vol. 31, no. 11, pp. 1279–1291, 2012.

[43] R. E. Burkard, "Selected topics on assignment problems," *Discrete Appl. Math.*, vol. 123, nos. 1–3, pp. 257–302, 2002.

[44] V. Isler and R. Bajcsy, "The sensor selection problem for bounded uncertainty sensing models," *IEEE Trans. Autom. Sci. Eng.*, vol. 3, no. 4, pp. 372–381, Apr. 2006.

[45] A. I. Mourikis and S. I. Roumeliotis, "Optimal sensor scheduling for resource-constrained localization of mobile robot formations," *IEEE Trans. Robot.*, vol. 22, no. 5, pp. 917–931, Oct. 2006.

[46] Y. Mo, R. Ambrosino, and B. Sinopoli, "Sensor selection strategies for state estimation in energy constrained wireless sensor networks," *Automatica*, vol. 47, no. 7, pp. 1330–1338, 2011.

Fabio Morbidi (S'07–A'09–M'12) received the M.S. degree in computer engineering and Ph.D. degree in robotics and automation from the University of Siena, Siena, Italy, in 2005 and 2009, respectively.

He was a Visiting Scholar with the Center for Control, Dynamical Systems and Computation, University of California, Santa Barbara, for six months from 2007 to 2008. He was a Post-Doctoral Researcher with the University of Siena, Northwestern University, Evanston, IL, and the University of Texas at Arlington, from January 2009 to August 2011. Since September 2011, he has been a Faculty Member with the Institute for Design and Control of Mechatronical Systems, Johannes Kepler University, Linz, Austria. His current research interests include multi-agent systems, formation control, robot vision, and geometric control.

Gian Luca Mariottini (S'04–M'06) received the M.S. degree in computer engineering and Ph.D. degree in robotics and automation from the University of Siena, Siena, Italy, in 2002 and 2006, respectively.

He was a Visiting Scholar with the GRASP Laboratory, CIS Department, University of Pennsylvania, Philadelphia, in 2005 and 2007. He was a Post-Doctoral Researcher with the University of Siena from 2006 to 2007, the Georgia Institute of Technology, Atlanta, from 2007 to 2008, and the University of Minnesota, Minneapolis, from 2008 to 2010. Since 2010, he has been an Assistant Professor with the Department of Computer Science and Engineering, University of Texas at Arlington, where he directs the ASTRA Robotics Laboratory. His current research interests include robotics and computer vision, with a particular focus on single- and multi-robot sensing, localization, and control, as well as on surgical vision and augmented reality systems for minimally invasive surgical scenarios.